Applied Geochemistry 206 (2026) 106921

Contents lists available at ScienceDirect

Applied Geochemistry

journal homepage: www.elsevier.com/locate/apgeochem

A multi-proxy perspective on stream sediment provenance and anthropogenic impacts in an ore-exploited, geologically complex river basin

Francesca Giannetti [a,b,*], Caterina Gozzi [a,b], Gerd Rantitsch [c], Stefania Venturi [a,b], Riccardo Avanzinelli [a,d], Robert Scholger [c], Claudio Natali [a,e], Giovanni Orazio Lepore [a], Marta Morana [a], Valentina Rimondi [a,b], Antonella Buccianti [a,b,f]

[a] University of Florence, Department of Earth Sciences, Via G. La Pira 4, Firenze, 50121, Italy
[b] NBFC, National Biodiversity Future Center, Palermo, 90133, Italy
[c] Department of Applied Geosciences and Geophysics, Montanuniversität Leoben, Peter Tunner Strasse 5, Leoben, 8700, Austria
[d] CNR, Institute of Geoscience and Georesources, Via G. La Pira 4, Firenze, 50121, Italy
[e] CNR, Institute of Environmental Geology and Geoengineering, Via Salaria Km 29,300, Montelibretti, 00015, Italy
[f] National Centre for HPC, Big Data and Quantum Computing, PNRR, Italy

ARTICLE INFO

Editorial handling by: Elisa Sacchi

Keywords:
Isometric log-ratio transformation
Sequential binary partition
Compositional data analysis
Stream sediments
Anthropogenic impact
Sediment geochemistry

ABSTRACT

Stream sediments integrate the geochemical and mineralogical signals of entire drainage basins, reflecting both bedrock lithology and anthropogenic inputs. This study applies knowledge-driven Sequential Binary Partitions (SBPs) of isometric log-ratio (ilr)-transformed data to unravel relationships among geochemistry, mineralogy, and mass-specific magnetic susceptibility (χ), with an approach tested on a representative river basin (i.e., Ombrone Grossetano River Basin, Southern Tuscany, Italy), lithologically diverse and impacted by past mining activities. The method aims to improve the understanding of natural and anthropogenic influences on sediment composition. Geochemical data (X-ray fluorescence) were transformed through ilr-balances, whereas mineralogical compositions (X-ray diffraction), lithological information, and χ measurements were used to support the interpretation of sediment sources. Strong correlations between ilr-balances and mineral phases confirm that the geochemical signals reliably reflect sediment mineralogy and the basin's lithological variability. Comparisons between χ and ilr-balances detect localized anthropogenic inputs, notably Fe-enrichments linked to historical mining in a specific sub-basin (Farma-Merse). The combined use of compositional data analysis, mineralogical constraints and magnetic susceptibility provides a transferable framework to investigate sediment provenance and anthropogenic legacy in complex river systems. Beyond the case study, the results highlight the importance of considering whole-composition geochemical relationships to correctly interpret element distributions in fluvial sediments.

1. Introduction

Stream sediments result from diverse contributions of an entire drainage basin, giving information on the lithological composition of the bedrock, mineralization and eventual contamination within the catchment (Halamić et al., 2001; Reimann and Melezhik, 2001; Xie et al., 2010; Wang et al., 2022). The mineralogy and geochemistry of sediment samples are closely linked; however chemical elements may be distributed among various minerals, both major and accessory, leading to potential misinterpretations if isolated elemental abundances are considered (Griffioen et al., 2025). Therefore, it becomes crucial to study not only the chemical composition of stream sediments, but to consider their mineralogical composition as well.

Geochemical datasets from stream sediments are compositional data, as their parts are positive and constrained to a constant sum (Aitchison, 1986) and pertain to a sample space called *simplex* (Pawlowsky-Glahn and Egozcue, 2001). To move out of the *simplex* and to be able to analyse data using classical statistical techniques, data need to be

* Corresponding author. University of Florence, Department of Earth Sciences, Via G. La Pira 4, 50121, Firenze, Italy.
E-mail address: francesca.giannetti1@unifi.it (F. Giannetti).

https://doi.org/10.1016/j.apgeochem.2026.106921
Received 19 February 2026; Received in revised form 28 April 2026; Accepted 3 June 2026
Available online 3 June 2026

transformed (Egozcue et al., 2003; Pawlowsky-Glahn et al., 2015).

An isometric log-ratio (ilr) transformation (Egozcue et al., 2003) with balances derived from a Sequential Binary Partition (SBP; Egozcue and Pawlowsky-Glahn, 2005) enables a holistic view of the geochemical landscape of stream sediments. Recent applications in environmental and exploration geochemistry show that knowledge- or data-driven SBPs yield balances that sharpen anomaly patterns and improve interpretability in stream surveys (Liu et al., 2020; Gozzi et al., 2024;Gozzi, 2025).

As major element ratios are strongly constrained by mineral stoichiometry, ilr-balances bridge bulk chemistry to mineralogy. Consequently, the combination of ilr and mineralogy assesses the influence of the basin lithology.

In this study, we apply a CoDA (Compositional Data Analysis)-based approach by building knowledge-driven SBPs of ilr-transformed data of stream sediment compositions and combine it with the distribution and morphology of ferrimagnetic minerals (e.g., magnetite). These minerals control mass specific magnetic susceptibility (χ), which serves as an independent physical proxy evaluating possible anthropogenic contributions (e.g. Scholger, 1998; Schmidt et al., 2005; Faměra et al., 2018).

Three main objectives are addressed: (i) to chemically characterize sediments of a geologically heterogenous river basin and identify the dominant compositional patterns; (ii) to link these patterns to mineralogical phases, thereby linking geochemistry and mineralogy, and (iii) to evaluate the potential of χ as a complementary proxy for both lithological variability and anthropogenic influence. This approach assesses the extent to which SBPs balances can be used to unify geochemical, mineralogical and physical proxies into a single interpretive framework.

The study area is given by the Ombrone Grossetano River Basin (OGRB), in Southern Tuscany (Italy), characterized by lithologically diverse domains. The OGRB is also an important metallogenic province where a wide variety of metal resources have been exploited for almost three millennia (Dini, 2003). To the west of the OGRB, the pyrite and Cu–Pb–Zn-(Ag) ores of the Colline Metallifere district have been exploited up until the 1990s, when the last pyrite mine (Campiano) was shut down (Dini, 2003). To the east, the Monte Amiata region was exploited for over a century as one of the major mercury producers in the world due to its cinnabar-rich ore deposits, with associated pyrite and marcasite (Dini, 2003). The OGRB is located between these two districts, possibly being impacted by both and by the related anthropogenic activities (i.e., mining activities). Indeed, the basin, particularly the Farma–Merse sub-basin, shows the evidence of past mining activities, with abandoned mining sites and mine wastes that may still influence sediment geochemistry and, subsequently, the entire river ecosystem. However, the wide range of lithologies also contributes naturally to metal concentrations, making the OGRB a suitable case study for disentangling natural geochemical backgrounds from anthropogenic inputs. Today, agriculture dominates the region and represents its primary land use (Diodato et al., 2023).

2. Materials and methods

2.1. The Ombrone grossetano river basin

2.1.1. Hydrographic setting, climate and land use of the river basin

The Ombrone grossetano (hereafter indicated as Ombrone River) is

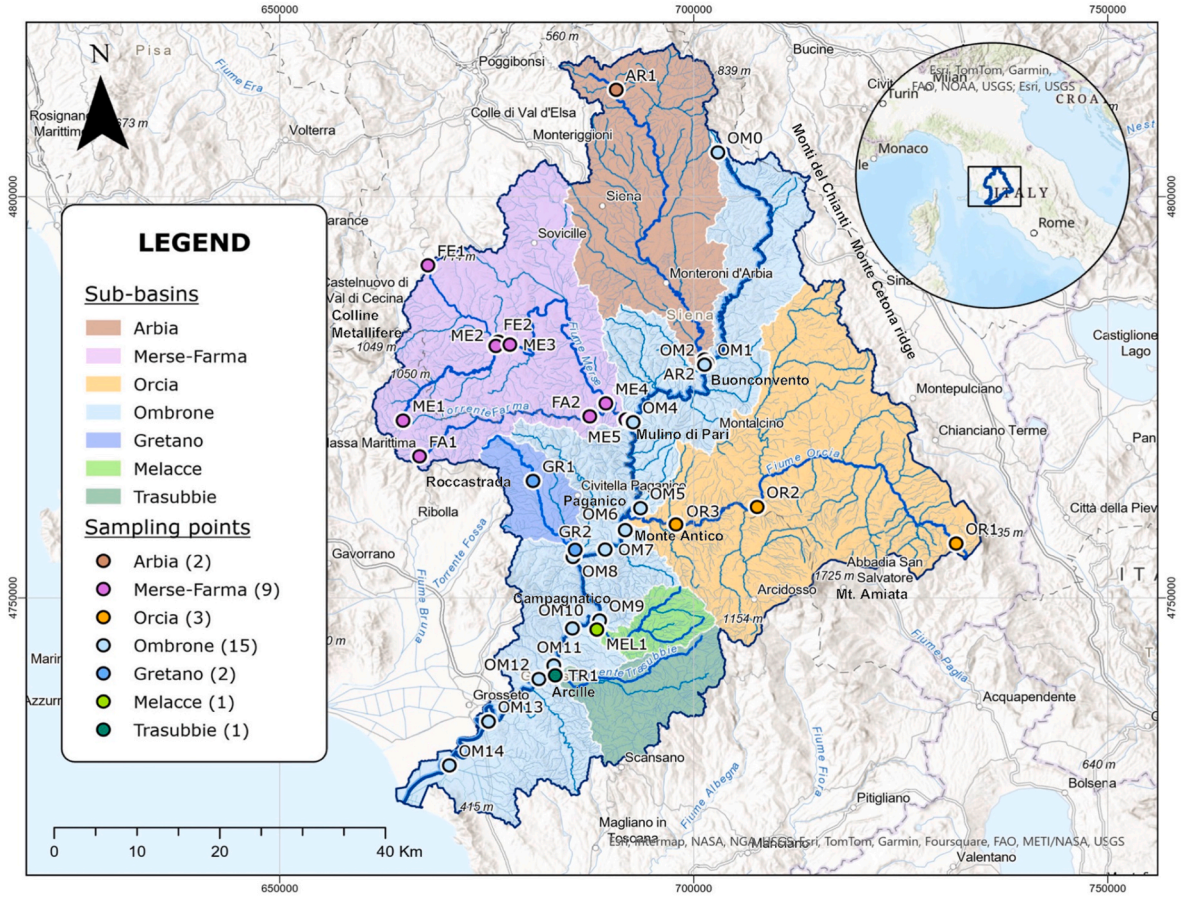

Fig. 1. Map of the Ombrone River Basin showing the defined sub-basins and the locations of the stream sediment sampling points. OM = Ombrone River; OR = Orcia River; MEL = Melacce Creek; TR = Trasubbie Creek; GR = Gretano Creek; ME = Merse River; FA = Farma Creek; FE = Feccia Creek; AR = Arbia River. Samples have been named based on the first two letters of the name of the watershed (except for Melacce, where three letters were used to avoid confusion with the Merse samples), with an increasing Arabic number going from the spring to the mouth of the waterways (e.g., ME1 = upstream, ME5 = downstream).

the main river of the OGRB, which spans an area of 3494 km^2 in Southern Tuscany, Italy (Fig. 1). The main river originates in the Apennines and flows for approximately 161 km before reaching the Tyrrhenian Sea. It is the second-longest river in Tuscany; however, due to the high erodibility of the lithologies underlying its course, the Ombrone River exhibits the highest suspended sediment load (Frangipane and Paris, 1994; Diodato et al., 2023).

The Ombrone River receives six major tributaries (Fig. 1). On its hydraulic right, it is fed by (i) the Arbia River (63.5 km), originating in the Monti del Chianti and joining the main river in Buonconvento (Siena), (ii) the Merse River (71 km), draining the Colline Metallifere and receiving the Farma and Feccia creeks before flowing into the Ombrone River near Mulino di Pari (Cavalieri, 2001), and (iii) the Gretano Creek (25 km), flowing from Roccastrada to Paganico. On its hydraulic left, it receives (i) the Orcia River, which represents the largest tributary (50 km), draining the northern side of Monte Amiata and entering the Ombrone at Monte Antico (Grosseto), and the (ii) Melacce and (iii) Trasubbie creeks, that flow for 16 and 28 km before joining the Ombrone River at Campagnatico and Arcille, respectively.

Out of these, the Merse (and its tributary Farma) and Orcia rivers are of extreme importance. The former drains an area affected by mining activities that took place since the 16th century AD at least (Benvenuti et al., 1997). The latter drains an area that is relatively devoid of anthropogenic pressures, except for the presence of part of the Hg mines pertaining to the Monte Amiata complex (Dini, 2003); however, in recent years this area has been affected by dredges and high-rate draining for intensive crops (Cavalieri, 2001).

According to the Köppen classification (Köppen, 1931), the OGRB is characterized by a hot-summer Mediterranean (Csa) climate, characterized by hot, dry summers and cool, wet winters, with annual precipitation ranging from 600 to 1100 mm (Beck et al., 2018; Villani et al., 2024). The most internal part of the basin displays greater precipitation and shorter summers (Diodato et al., 2023).

Land use and coverage of the OGRB include forest (39%), herbaceous annual crops (46.9%), permanent pastures (4.3%), vineyards and olive groves (respectively, 3.8% and 1.9%) and 4.1% covered with artificial surfaces, shrubland and bare land (Villani et al., 2024).

2.1.2. *Geological and lithological characteristics of the basin*

The OGRB lies in Southern Tuscany, on the southernmost edge of the Northern Apennines, a late Cretaceous (Upper Cretaceous-Upper Oligocene; e.g., Martini and Sagri, 1993; Carmignani et al., 1994) collisional belt. The crustal extension that began during the Upper Miocene (Carmignani et al., 1994; Bonciani et al., 2005; Brogi et al., 2005) resulted in the continental lithosphere thinning and development of horst and graben structures, with continental and marine sediments filling the basins (Martini and Sagri, 1993; Brogi and Liotta, 2008; Cornamusini et al., 2011). Both mantle-derived volcanism (from Miocene to Pleistocene; Conticelli et al., 2010 and reference therein) and crustal-derived igneous intrusions and volcanism (Miocene – Pliocene; e.g., Dini et al., 2005, 2008; Marroni et al., 2015 and reference therein) characterized this extensional phase.

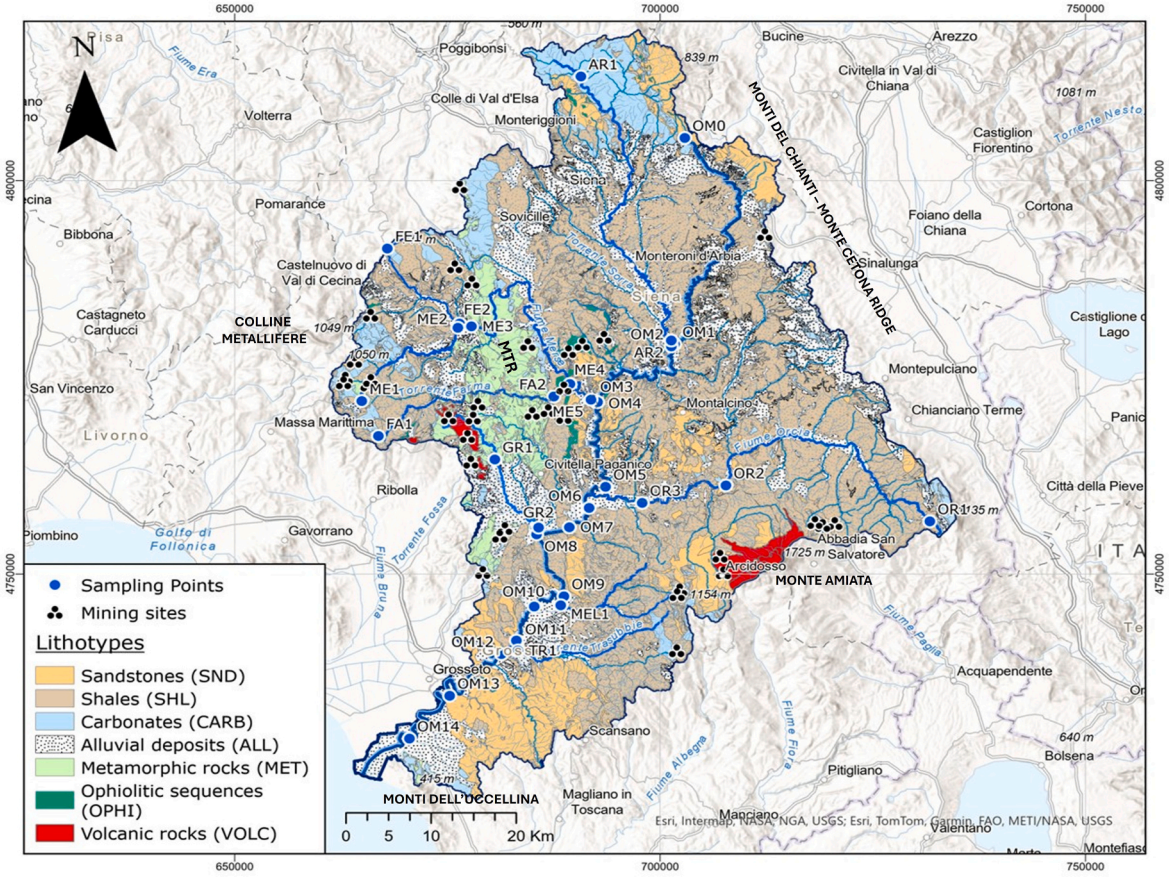

Fig. 2. Simplified lithological map of the Ombrone River Basin. Main lithologies have been inferred from Regione Toscana (2022b). Sandstones (SND): Sandstones, turbiditic sandstones, siliciclastic turbidites. Shales (SHL): Clay, silty and marly clays, shales, marls, calcilutites, siltstones. Carbonates (CARB): Limestone, dolomitic limestone and dolomite, flysch, marly limestone. Alluvial deposits (ALL): Sands, pebbles, muds, travertines and continental limestones. Metamorphic rocks (MET): Metamorphic limestones, dolomitic metacarbonates, quartzites, phyllites, quartzose metaconglomerates. Ultramafic rocks (OPHI): Ophiolitic breccias, serpentinized peridotites. Volcanic rocks (VOLC): Volcanic rocks, pyroclastic rocks. MTR = Middle Tuscan Ridge. Location of mining site and mineral resources from the DB_RIMI (Regione Toscana, 2012) is also reported.

Within this geodynamic framework, the OGRB overlies four Tuscan basins (the Siena – Radicofani graben to the northeast, the Radicondoli – Chiusdino graben to the west, the Baccinello – Cinigiano and Velona graben on the southeastern side; Martini and Sagri, 1993; Pandeli, 2008), and is bordered to the eastern and northern sides by the Monti del Chianti - Monte Cetona Ridge and Monte Amiata, and by the Colline Metallifere to the west (Fig. 2). The Middle Tuscan Ridge (MTR) borders these structural basins and it is characterized by the presence of the metamorphic units of the Tuscan Sequence (Finetti et al., 2001, 2005 and references therein).

The area overlies tectonic units belonging to the Ligurian, Sub-Ligurian, and Tuscan domains (Carmignani et al., 1994, 2004; Finetti et al., 2001, 2005; Marroni et al., 2015), including ophiolitic, sedimentary, and metamorphic rocks. Taking into consideration the goals of this work, the main lithologies of the area pertaining to these domains have been summarized in Fig. 2 as follows: OPHI represents ophiolitic lithologies from the Internal Ligurian Domain, whereas the metamorphic rocks of the Tuscan Metamorphic Complex are referred to as MET. Calcareous-argillaceous and arenaceous sedimentary sequences from the Ligurian, Sub-Ligurian and Tuscan Domain are grouped in CARB, SHL and SND depending on the dominant component (i.e., respectively, carbonates, shales or sandstones). The upper Miocene-Quaternary magmatic bodies will be referred to as VOLC.

As shown in Fig. 2, SHL represents the predominant lithotype across the entire OGRB, particularly in the eastern sector, where it dominates the Orcia, Melacce, and Trasubbie sub-basins, as well as most of the Ombrone River's course. Moving southward toward the river's mouth, SND becomes increasingly dominant, especially downstream of the Trasubbie confluence. SND also occurs in the northern part of the basin, affecting the spring of both the main river and the Arbia tributary. On the western side, CARB lithotypes are common, particularly in the spring areas of the Arbia, Feccia, Farma and Merse watersheds. The Farma-Merse and Gretano sub-basins are instead characterized by MET and OPHI. VOLC are scattered throughout the basin but are prominent in the Gretano and Orcia (Monte Amiata) sub-basins.

2.1.3. Ore mineralization within the OGRB

The OGRB is located between various mineral belts (Fig. 2 and S1 in Supplementary Figures): the north-western side of the basin hosts a "Cu–Pb–Zn(-Ag) Zone", whereas the south-eastern side is bordered by the Hg metallogenic belt of Monte Amiata (Orcia sub-basin). The "Sb–Au Zone" district lies within the basin centre, and the "Pyrite Zone" borders the south-western side of the basin (Dini, 2003 and references therein). The river basin hosts various ores (locations are displayed in Fig. 2), whose exploitation began during the Etruscan period (Cipriani and Tanelli, 1983) and continued through the 19th century. Nowadays, extraction is limited to ornamental stones, building materials and a few industrial minerals (Dini, 2003; Regione Toscana, 2022a). Pyrite was the most extensively exploited resource, particularly in the Farma-Merse sub-basin, yielding ca. 100 Mt of ore until the closure of the Campiano Mine in the 1990s (Dini, 2003). This sub-basin also hosts Cu–Zn volcanogenic massive sulfides, Carlin-type Au and Sb deposits associated with the Calcare Cavernoso and geothermal systems of the Middle Tuscan Ridge (Dini et al., 2024). On the other side, the Orcia sub-basin hosts a small portion of the supergiant Monte Amiata Hg district, which as a whole accounted for 10% of Hg world production prior to the closure of the mines (Dini, 2003; Dini, 2017). However, stream sediment surveys in the Orcia and Ombrone rivers indicate that Hg and As concentrations rarely exceed Italian environmental quality standards, with anomalous values restricted to the immediate vicinity of former mine sites (Chiarantini et al., 2016). At present, the input of these elements into the watershed does not pose an immediate environmental threat to the broader basin. However, minor occurrences of Cu, Pb, Fe, Mn, and Sb are widespread throughout the basin (Dini, 2003). Despite the end of majority of mining activities, their environmental impact persists, as abandoned waste rock dumps, flotation tailings, and acid mine drainage have locally impacted water quality, particularly in the Farma-Merse sub-basin (Benvenuti et al., 1997; ARPAT, 2014, 2017; Monaci et al., 2021).

2.2. Methods

2.2.1. Sampling strategy and analytical methods

A total of 33 sediment samples of the Ombrone river and its major tributaries was collected during the spring 2023 (Figs. 1 and 2). Despite the relatively limited number of samples compared to the extent of the study area (ca. 3500 km^2), the adopted sampling strategy was designed to capture the main lithological contrasts within the basin, with a higher sampling density in the more heterogeneous western sector of the OGRB. Due to the homogeneity of the lithologies and the virtual absence of anthropic pressures, the Trasubbie and Melacce sub-basins have only been sampled in one point toward the mouth of the waterways.

The sediments were dried at 40 °C in a ventilated oven; then, two different aliquots were separated, one sieved at 180 μm (aliquot "A") and one at 2 mm (aliquot "B"). With reference to the Wentworth (1922) grain size classification, the <2 mm fraction encompasses coarse to fine sand (63–2000 μm), silt (4–63 μm) and clay (<4 μm), whereas the <180 μm fraction includes fine to very fine sand (63–180 μm), silt (4–63 μm) and clay (<4 μm). Although a full granulometric analysis was not performed in the present study, this latter fraction is expected to be dominated by silt- and clay-sized particles.

The <180 μm fraction (aliquot A) was selected due to the preferential distribution of trace elements in finer sediments (e.g., Wilber and Hunter, 1979), which are a major sink of metals (e.g., Frankowski et al., 2008). The <180 μm (or <80 mesh) fraction is furthermore widely adopted in sediment geochemical studies, with application in several regional surveys (e.g., Dinelli et al., 2005; Gray et al., 2014; Chiarantini et al., 2016). Frankowski et al. (2008) further showed that heavy metal enrichment is significant not only in the <63 μm fraction but also in the 63–100 μm range, reinforcing the appropriateness of the <180 μm cut-off when dry-sieving methods are employed, as was the case in the present study.

Although Italian legislation does not provide specific guidelines for sediment analysis, the D. Lgs 152/06 references to concentration of elements and compounds in soils sieved at 2 mm (aliquot B), hence the selection of this grain size.

Samples were then milled and homogenized for 20-40 min using an agate planetary ball-mill (Fritsch Pulverisette 5), to obtain the powder used for all analyses described hereon. Both aliquots have been subjected to the same analyses.

The determination of Loss on Ignition (LOI) was performed by gravimetric method: powders were dried overnight at 105 °C, and then 3 g were subjected to calcination at 1050 °C for 2 h. Major, minor (SiO_2, Al_2O_3, CaO, K_2O, Na_2O, Fe_2O_3, MnO, MgO, TiO_2, P_2O_5) and trace elements (V, Ga, Rb, Cu, Zn, Sr, Zr, Ba) were analysed using a PANalytical Axios XRF Spectrometer on beads made with $Li_2B_4O_7$. XRF calibration was performed using GeoPT standards from the International Association of Geoanalysts, covering the necessary wide range of concentrations (Webb et al., 2022). Both LOI and XRF measures were carried out at the Montanuniversität Leoben laboratories, Chair of Geology and Economic Geology.

Mass specific magnetic susceptibility (χ) has been tested as an indicator for heavy metal contamination of river sediments (Scholger, 1998), adding useful information to the chemical analysis at low cost and in a short time. The bulk χ was measured at the Paleomagnetic Laboratory of the Chair of Applied Geophysics of the Montanuniversität Leoben in Gams (Frohnleiten, Austria) with an error <1% by means of a Multifunction Kappabridge (Agico MFK1-FA) with a field strength of 200 A/m and a frequency of 976 Hz. For each sample, about 10 g of powdered sediment were weighted and filled in plastic cylinders of 10 cm^3 for the measurements. Magnetic particles from selected non-powdered samples were retrieved using a hand magnet; these were

later observed with a digital microscope to gather information on their morphologies. Raman spectra of these high χ samples were collected with a Horiba Labram HR Evolution, supplied with a 100 mW Nd:Yag (532 nm) laser, a confocal microscope (100× objective with a 0.80 numerical aperture and a confocal hole aperture of 100 μm) and a 1800 g/mm grating; a Peltier cooled CCD detector was used to collect Raman spectra. The wavenumbers were calibrated using the Rayleigh scattering line (0 cm^{-1}) and a silicon wafer standard (520.7 cm^{-1}). Mineral identification was carried out based on diagnostic Raman bands and comparison with reference spectra from the RHX database. Magnetite was identified based on its characteristic peak at ~670 cm^{-1}, whereas serpentine was recognized through its typical band at ~690 cm^{-1}. These peak positions are consistent with those reported in literature (e.g., Shebanova and Lazor, 2003; Auzende et al., 2004), and the spectra match the ones from the RHX database, therefore these peaks and their relative intensity patterns were used as the criteria for confirming mineral identification. Spectra can be found in Supplementary Figures (Fig. S2).

Qualitative and semi-quantitative mineralogical composition was determined via X-ray powder diffraction (XRPD) at the Centro di Servizi di Cristallografia Strutturale (CRIST) of the University of Florence. Data collection was performed using an Anton Paar XRDynamic 500 diffractometer with a Co Kα radiation (1.7902 Å). The measured 2θ interval ranges from 3 to 90° with a step size of 0.02° and an exposure time of 30 s. The sample holder was kept spinning during the measurements in order to reduce preferred orientation effects. Phase identification was conducted using DIFFRAC. EVA (Bruker) and the Crystallography Open Database (Vaitkus et al., 2023). Semi-quantitative analysis was performed using TOPAS (Coelho, 2018).

2.2.2. Watersheds delineation

To map the influencing upstream area of the samples, watersheds were defined for each sampling point using ArcGIS Pro software (Esri, 2025a). Each sediment sampling point defines the pour point (outlet) of its corresponding contributing area.

The watersheds were delineated from the 10 m resolution Hydrographic Digital Terrain Model (HDTM) provided by the Tuscany Region (Directorate of Urban Planning and Housing Policies - Department of Territorial and Environmental Information Systems; Regione Toscana, 2021), optimized for use in hydrological models. The *Hydrology* and *Spatial Analyst* tools in ArcGIS were applied to first fill any depressions in the HDTM and then calculate the flow direction and accumulation. This sequence of steps allowed for the accurate determination of the contributing area for each watershed (Fig. S3 in Supplementary Figures). To estimate the extent of the areas covered by the different outcropping lithologies (Fig. 2) for each watershed, the *Tabulate Area* tool was applied (Esri, 2025b).

2.2.3. Compositional data analysis (CoDA)

The understanding of geochemical data requires the use of compositional data analysis (CoDA) methods (e.g., Kirkwood et al., 2016; Gozzi et al., 2018, 2024). Compositional data represent the *D* parts of a whole and are constrained to a constant sum, therefore they are not free to have arbitrary values as there's the need to maintain the total sum (Aitchison, 1982, 1986). This kind of data is described by components that acquire information only when considered in relation to a reference (Egozcue et al., 2024), which is represented by the other components (*parts*) within the composition.

Moreover, compositional data pertain to a sample space called *simplex* (Pawlowsky-Glahn and Egozcue, 2001). The geometry of the *simplex* differs from Euclidean geometry. Since standard statistical tools are typically developed for the latter, it is necessary to apply specific transformations that move compositional data from the *simplex* to an unlimited space. These include the additive log-ratio (alr), the centred log-ratio (clr) and isometric log-ratio (ilr) transformations (Aitchison, 1986; Egozcue et al., 2003). The isometric log-ratio (ilr) transformation, as formulated by Egozcue et al. (2003), converts compositions into orthonormal coordinates in Euclidean space. Transformed data can then be analysed with the same tools as standard data (Egozcue et al., 2003).

To simplify the data analysis by using ilr coordinates, Egozcue and Pawlowsky-Glahn (2005) introduced the Sequential Binary Partition (SBP), which defines specialized ilr-transformed variables (i.e., balances) based on knowledge. Compositional data get divided in two groups, one standing as a numerator and one as the denominator of a log-ratio; then, both groups get, respectively, divided in two sub-groups, until all groups contain only one log-ratio with two parts. This sub-division can also be performed through data-driven methods such as hierarchical cluster analysis (e.g., Liu et al., 2018; Gozzi et al., 2024). This study adopted a knowledge-driven approach, grounded in the characteristics of the basin as described in Sec. 4, to better constrain the relationship between the data and the basin's features. All compositional data analyses were performed using the freeware CoDaPack (v. 2.03.01; Thió-Henestrosa and Martín-Fernández, 2005).

It is noteworthy that mineralogical data obtained from XRD analysis are also compositional data, as the relative abundances of mineral phases within each sample are constrained to sum to a constant (100%), and are therefore subjected to the same closure problem as geochemical data (Aitchison, 1986). However, mineralogical abundances are semi-quantitative data, and in this work they are used to evaluate whether the ilr-balances derived from geochemical data correlate with specific mineral phases. For this purpose, each mineral phase was expressed as the natural logarithm of the ratio of that phase to the sum of all other detected mineral phases [ln (mineral/Σ other minerals)], allocating the data outside of the simplex and making them suitable for standard correlation analysis (Spearman's ρ), necessary for the method validation (see Sec. 4.2).

3. Results

3.1. Classic exploratory analysis

3.1.1. Grain size of stream sediment samples

As presented in Sec. 2.2.1, for each of the thirty-three stream sediment sampling points (fifteen for the main river Ombrone and eighteen for the major tributaries) two different aliquots were separated, a fine one sieved at 180 μm (aliquot "A") and a coarse one sieved at 2 mm (aliquot "B").

Considering the ratio between the two grain fractions, the sediment grain-size distribution in the OGRB (Table S1 Supplementary) varies along the river course. The ratio between the fraction <180 μm over the <2 mm one (%) ranges from as low as 2% (GR1) to as high as 82% (OM1). In all considered waterways there is no marked increase in the fine fraction going from spring to mouth, with the only exception of Arbia River. Among the tributaries, Gretano, Merse, Farma, Feccia, Melacce and Trasubbie display a higher proportion of coarse particles (>180 μm). On the contrary, the majority of the Arbia and Orcia samples have a higher proportion of the fine fraction (<180 μm). Considering the Ombrone River, more than half of samples display an A/B ratio of at least 50%, and the sediments that are the most enriched in the fine fraction lie upon the central part of the river basin. Indeed, a marked increase in the proportion of fine particles (<180 μm) in the Ombrone samples is evident at the confluence with the Arbia and Orcia rivers.

3.1.2. Mineralogical composition and mass specific magnetic susceptibility (χ)

Results for XRD on A and B-fractions of the OGRB stream sediments are presented through a Quartz – Calcite – Phyllosilicates ternary plot (Fig. 3a), combined with a lithological sketch map to highlight the mineralogical composition (Fig. 3b; Supplementary Table S1).

Across the basin, there are no major differences between the fine (A) and coarse (B) fractions (Fig. 3a and b). Quartz is the dominant phase in

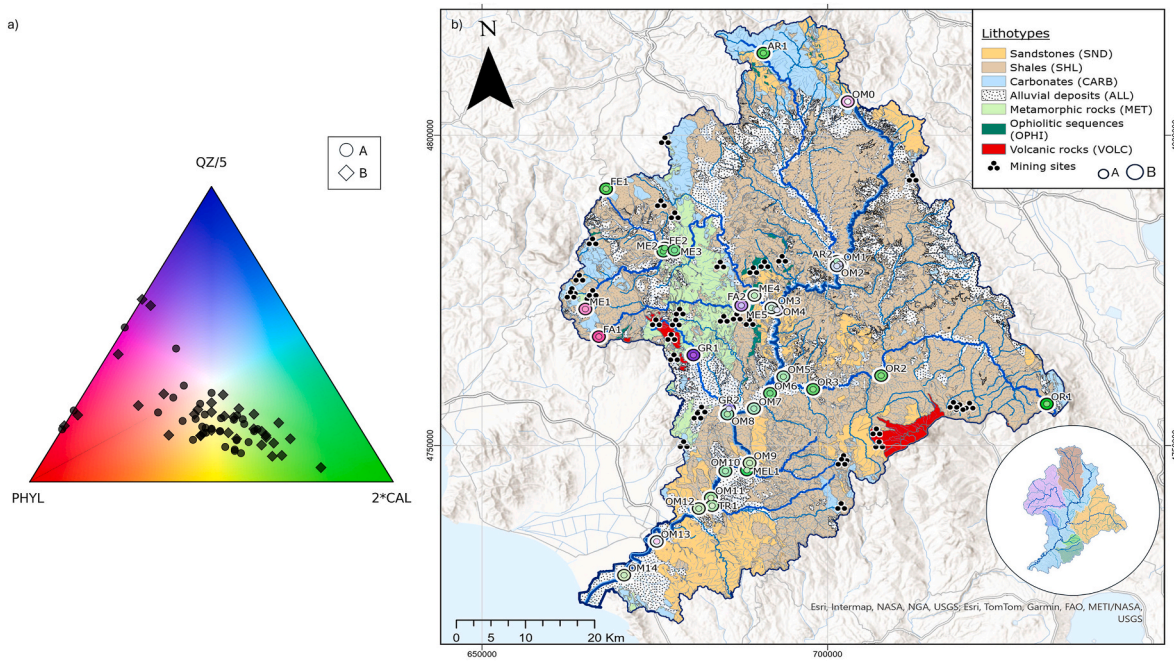

Fig. 3. a) QZ/5 – 2*CAL – PHYL ternary plot of sediments of both grain sizes (<180 μm and <2 mm) of the Ombrone basin; the background colour scheme was applied following the procedure described by Peeters (2014). QZ = quartz; CAL = calcite; PHYL = phyllosilicates. b) Samples have been coloured using the RGB from the plot on the left. For each sampling point, the larger symbol corresponds to the B-aliquot (<2 mm), whilst the smaller symbol depicts the A-aliquot (<180 μm). A sketch map with the main lithologies and mining sites of the area from the DB_RIMI (Regione Toscana, 2012) has been used to infer possible influences on the sediments' mineralogical composition, whilst the sub-basins are highlighted in the right corner. (For interpretation of the references to colour in this figure legend, the reader is referred to the Web version of this article.)

both the Ombrone samples and its major tributaries (except for OR1B) and it ranges from 25 to 89%. Its content reaches up to 89% in coarse fractions from the Gretano basin and remains high (>60%) in many Ombrone samples. There is a general decreasing trend in quartz contents from spring to mouth along the main river. Plagioclase, which represents a generally minor component (<10%) compared to quartz, behaves similarly.

Micas are the second most abundant phase in most samples (ranging from 7 to 43%): their concentration increases downstream and it is slightly higher in aliquots of the fine fraction (A), reaching values as high as 43% (Farma Creek). Mica-rich samples derive especially from tributaries such as Melacce, Feccia, Farma, Merse and downstream the Ombrone River.

Calcite content varies significantly across the basin from traces (<3%) to its maximum values in samples such as OR1B (40%, where it represents the most abundant phase), FE1B (31%), AR1B (30.2%) and MEL1B (26%). Calcite represents the second most abundant phase in samples from Feccia, Arbia and all the tributaries on the hydraulic left (i.e., Orcia, Melacce and Trasubbie).

Samples enriched in calcite were retrieved in areas where the main outcropping lithologies are represented by CARB, SHL and SND (Fig. 3a and b). Sediments from the spring of Merse and Farma are the only exception, as they lie on CARB but are almost devoid of calcite (ME1 only contains minor amounts of dolomite, near or below 3%; Supplementary Table S1) and heavily enriched in phyllosilicates. Samples lying on MET (FA2, GR1 and GR2) are depleted in calcite and enriched in quartz (Fig. 3a and b).

Chlorite-group minerals are consistently present across the dataset, displaying similar concentrations (6-12%) regardless of the sampling area, except for Feccia (FE), Gretano (GR) and a sample from Arbia (AR1B) where these minerals display low concentrations (<3%) or are not detected. The highest abundances are observed at the confluence between Farma and Merse (ME4B = 18%). Their presence is often coupled with increased mica content.

Dolomite is rare but present in significant amounts (>3%) in samples from Farma, Feccia, Merse and Orcia waterways where it ranges from 4% to 12%.

The results of χ measurements (Supplementary Table S1 and Fig. S4 in Supplementary Figures) range from 6.74×10^{-8} m^3/kg to 197×10^{-8} m^3/kg. The two analysed grain-size fractions are slightly different: the coarser fraction (<2 mm) shows a broader distribution, with a higher maximum value (197×10^{-8} m^3/kg), as well as a greater density of samples toward higher χ values compared to the finer fraction (<180 μm), suggesting that magnetic minerals are preferentially concentrated in the coarser grains (>180 μm).

Considering both grain sizes, the highest χ values were measured in the samples retrieved from the Merse-Farma and Gretano sub-basins (Fig. 4). The Ombrone samples retrieved after the confluence with the Merse sub-basin (from OM4 onwards) are all higher in χ compared to those sampled before the confluence, showing a persistent influence of the magnetic minerals coming from this sub-basin.

Ferrimagnetic particles extracted from relatively high χ ($>80 \times 10^{-8}$ m^3/kg) samples show morphologies compatible with a natural origin (Fig. S2 Supplementary Figures). Raman spectra collected on these particles identify magnetite and serpentine, as detailed in Sec. 2.2.1. No magnetite has been detected by XRD, consistent with the generally low χ measurements.

3.1.3. *Stream sediments chemical composition*

The results obtained from the XRF analysis are displayed in Supplementary Table S1. Major elements are expressed in wt.% whereas trace elements are in ppm. The median values for each sub-basin are reported in Table 1.

Median element concentrations from the two grain sizes (Fig. 5) are similar (Supplementary Table S1 and Table 1). However, Al_2O_3, P_2O_5, TiO_2, Zr, V and Rb are slightly enriched in the fine fraction; in particular, TiO_2 and Zr display the widest difference in the median concentration between the two grain sizes.

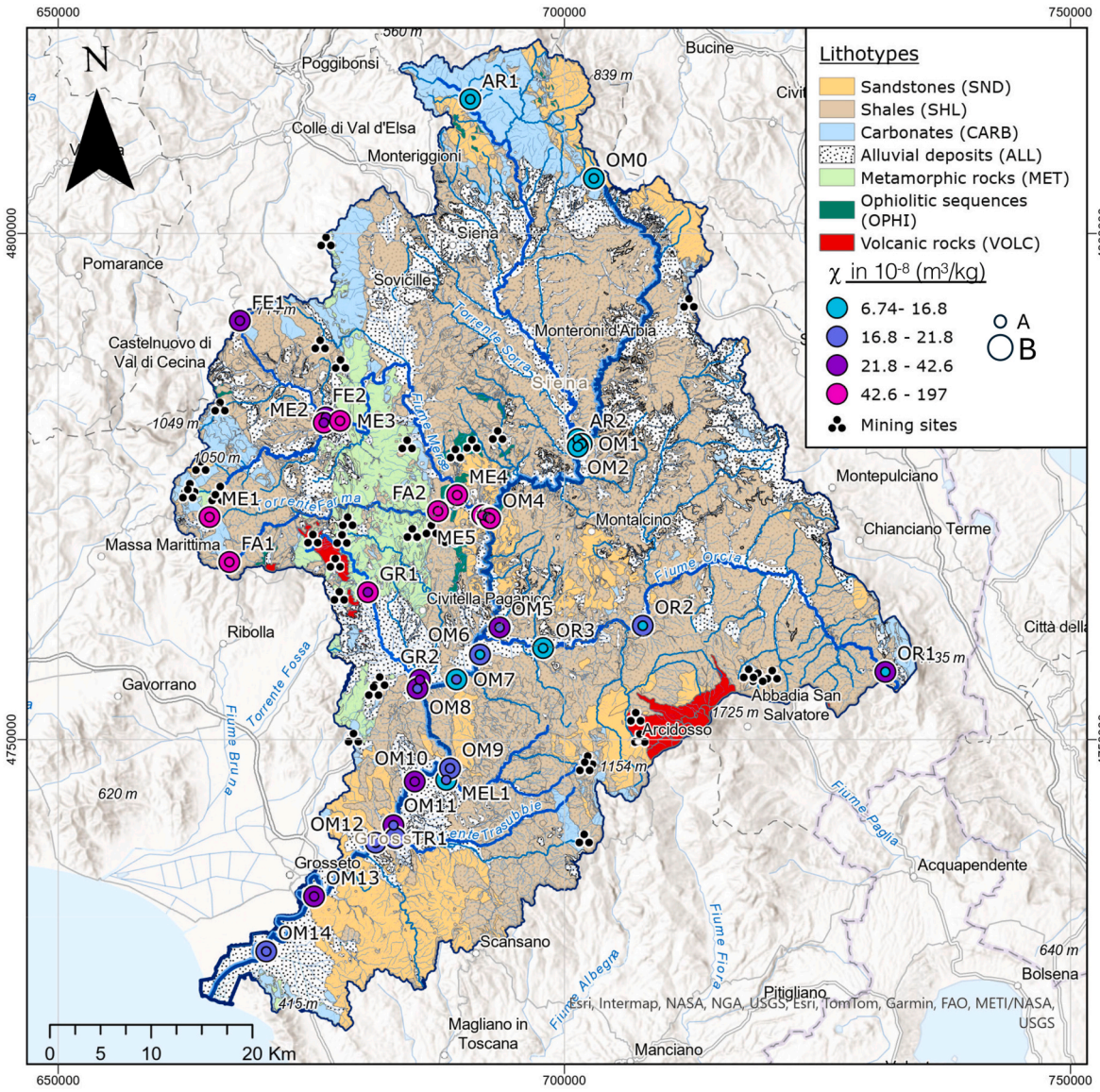

Fig. 4. Map depicting the values of Mass Specific Magnetic Susceptibility (χ in 10^{-8} m^3/kg) for both grain sizes; the larger symbols correspond to the B-aliquot (<2 mm), whilst the smaller symbols correspond to the A-aliquot (<180 μm). The location of mining sites from the DB_RIMI (Regione Toscana, 2012) is also highlighted.

Overall, the median Al_2O_3 of the OGRB is similar to that of the FOREGS geochemical baselines for European sediments (Salminen et al., 2005). The OGRB sediments are significantly enriched in CaO, Fe_2O_3 MgO, MnO, Cu and Sr and less enriched in Rb, V, Zn and Ga with respect to the reference median composition. On the contrary, the OGRB sediments show a slight depletion in SiO_2, K_2O, Na_2O, TiO_2, P_2O_5, Ba and Zr compared to FOREGS baselines.

The comparison of the stream sediment composition among different sub-basins with that of the entire OGRB, regardless of the samples' grain size (Table 1), highlights some peculiar local geochemical features (Fig. 6): Arbia samples are the most enriched in Na_2O (1.14 wt%), P_2O_5 (0.16 wt%) and Ba (389 ppm) compared to sediments from the other sub-basins; Farma-Merse samples are characterized by the highest Fe_2O_3 (6.06 wt%), Cu (54 ppm) and Zn (109 ppm) contents of all considered tributary basins; Orcia sediments are the most depleted in SiO_2 (46.6 wt %) and the most enriched in CaO and Sr (15.0 wt% and 338 ppm, respectively); Gretano samples are the most enriched in SiO_2 (78.9 wt%) and K_2O (2.15 wt%), whilst being the most depleted in CaO (1.76 wt%). CaO and Sr contents are also high in the Melacce samples (14.3 wt% and 316 ppm, respectively) with respect to sediments from the other sub-basins, whereas the highest Al_2O_3 contents are shown by the Trasubbie samples (12.0 wt%).

A ternary plot based on the three most abundant oxides in the investigated samples (their sum accounts for more than 50 wt% of the total composition) has been produced; the results in RGB colours are used to display samples on a lithological sketch map (Fig. 6).

Samples collected from SHL, SND and CARB lithological domains display a relatively high CaO concentration, with some exceptions represented by samples FA1 and ME1 that show instead a peculiar enrichment in Al_2O_3. This is in accordance with the mineralogical composition: these latter samples are characterized by high contents of phyllosilicates, whereas all the others do present relatively high calcite concentrations. Samples collected from MET sequences are enriched in SiO_2, in agreement with the high quartz contents, with the only exception of sample GR2 that displays a relatively high CaO content.

3.1.4. *Lithological composition of the catchments*

The lithological composition of the catchment areas (Table 2)

Table 1
Median values for the different sub-basins and for the whole basin (OGRB); *Median of the baseline values from European stream sediments are reported as reference; data do not take LOI into account (FOREGS; Salminen et al., 2005).

Median	Arbia	Farma-Merse	Orcia	Ombrone	Gretano	Melacce	Trasubbie	OGRB	FOREGS*
n. of values	4	18	6	30	4	2	2	66	
SiO_2 (wt.%)	53.2	55.4	46.6	61.1	78.9	52.7	58.1	56.9	61.3
TiO_2 (wt.%)	0.47	0.56	0.51	0.48	0.41	0.38	0.49	0.49	0.63
Al_2O_3 (wt.%)	10.1	10.6	11.1	10.6	8.49	9.49	12.0	10.53	10.3
Fe_2O_3 (wt.%)	3.86	6.06	5.23	4.39	3.29	4.98	5.16	4.87	3.57
MnO (wt.%)	0.13	0.17	0.14	0.11	0.07	0.18	0.15	0.12	0.08
MgO (wt.%)	1.12	1.69	1.96	1.63	0.37	1.44	1.62	1.61	1.2
CaO (wt.%)	12.8	9.08	15.0	9.24	1.76	14.3	9.34	9.43	2.33
Na_2O (wt.%)	1.14	0.47	0.67	1.12	0.65	0.67	1.03	0.83	0.9
K_2O (wt.%)	1.63	1.94	1.66	1.84	2.15	1.60	2.01	1.85	2.01
P_2O_5 (wt.%)	0.16	0.10	0.13	0.11	0.07	0.09	0.09	0.11	0.14
LOI (wt.%)	14.9	11.8	16.0	11.2	4.01	14.5	10.6	11.28	-
V (ppm)	73	80	85	70	52	62	82	73	62
Cu (ppm)	48	54	29	27	12	26	32	29	17
Zn (ppm)	75	109	85	73	41	80	84	80	71
Ga (ppm)	12	14	15	14	14	12	16	14	12
Rb (ppm)	74	81	70	76	110	65	81	79	70
Sr (ppm)	278	239	338	235	78	316	208	241	126
Zr (ppm)	161	119	113	146	155	87	104	128	391
Ba (ppm)	389	298	255	299	242	253	304	290	386

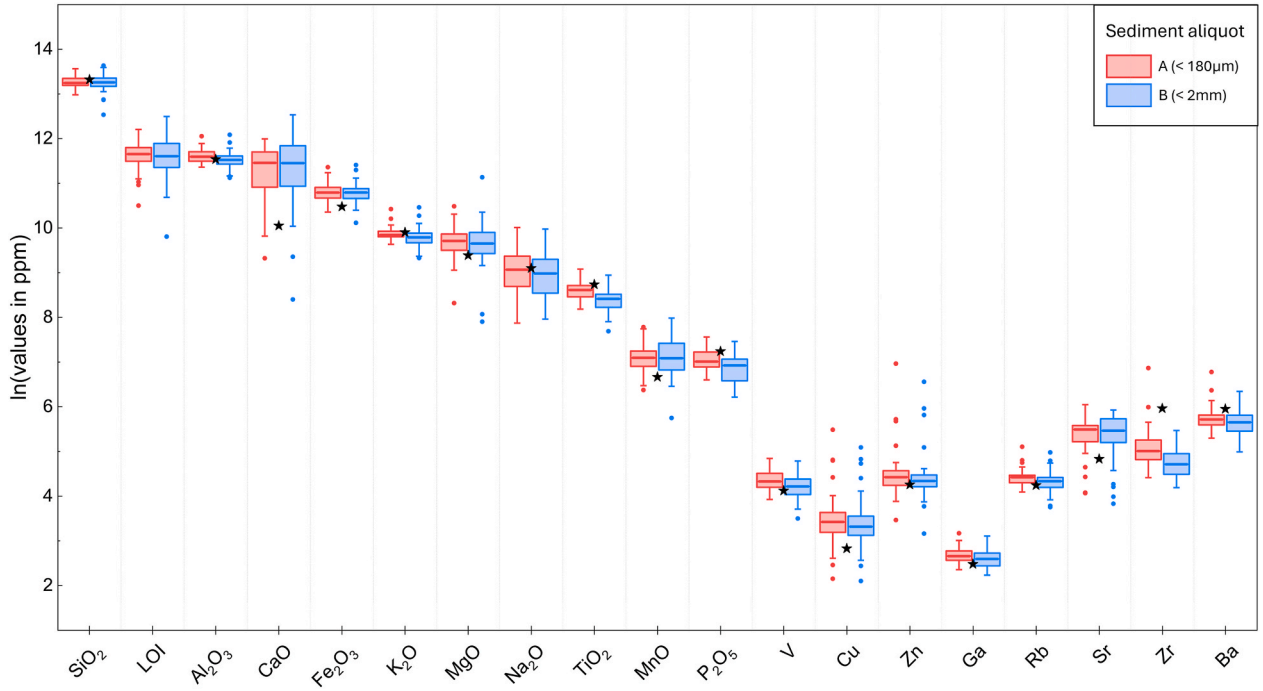

Fig. 5. Boxplots of the major and minor elements in the Ombrone basin (ln of values in ppm), showing the differences between the <180 µm (A) and <2 mm (B) aliquots. Median baseline values of these elements in European stream sediments (FOREGS; Salminen et al., 2005) are given as a reference (black stars).

associated with each sampling point was quantified as percentages of major lithological units as defined in Sec. 2.2.2 and Fig. 2.

Samples show a wide variability in catchment lithology, ranging from almost mono-lithological basins, such as Melacce (MEL1 = 78% SHL) or the spring of the Ombrone River (OM0 = 74% SND), to more heterogeneous ones with various contributions from multiple lithologies (e.g., OM4, OM10, OM14).

All calculated watersheds are primarily lying upon SHL, except for samples OM0 and AR1 where SND and CARB represent the major lithology, respectively, and Gretano samples that are majorly affected by ALL.

CARB affect primarily the Arbia and the spring of Ombrone, Feccia, Farma, Merse and Orcia. SND are present within the OM0, OM1, OM13 and OM14 watersheds, as well as TR1; in all other sampling points it represents less than 10% of the lithologies of the delineated watersheds. OPHI are present only in the western part of the basin, affecting primarily the Gretano, Farma and Merse waterways; these, together with the Orcia River, contain VOLC lithologies as well.

ALL contents show a marked variability too, covering more than 70% of the waterway of sample GR1 and only 2% in samples FA1, or not being present within the FE1 watershed.

4. Discussion

Stream sediments result from the physical-chemical weathering and erosion processes of the upstream lithologies and inputs related to human activities (e.g., mining). Their composition is therefore the result of natural and anthropogenic sources (Najafian et al., 2023 and

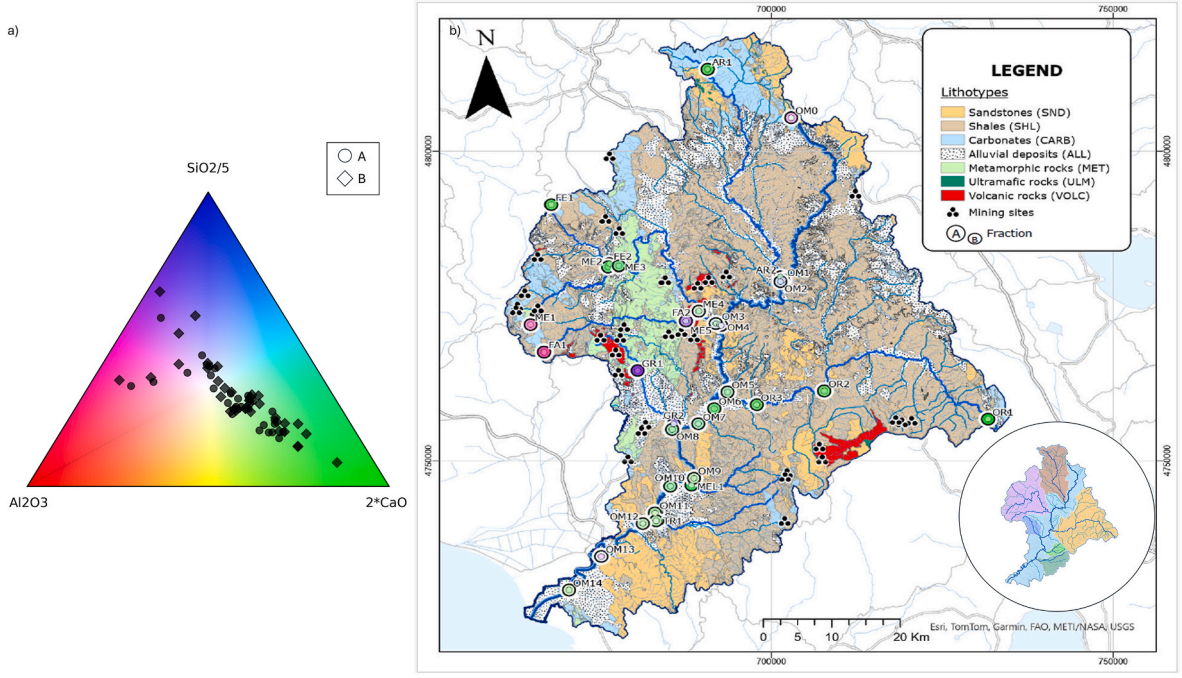

Fig. 6. a) $SiO_2/5 - 2*CaO - Al_2O_3$ ternary plot showing the major chemical composition of sediment samples of both aliquots; the background colour scheme was applied following the procedure described by Peeters (2014). b) Map highlighting the distribution of major elements in the samples, which are displayed using the RGB colours coming from the ternary plot on the left. A sketch map of the major lithologies within the basin has been used to infer the eventual influence of the lithologies on the chemical composition of sediments. The location of mining sites from the DB_RIMI (Regione Toscana, 2012) is also displayed. On the right corner, the sub-basins of the OGRB are highlighted. (For interpretation of the references to colour in this figure legend, the reader is referred to the Web version of this article.)

Table 2
Percentages of lithotypes affecting the delineated watershed of each sampling point.

SAMPLE	SHL (%)	CARB (%)	SND (%)	VOLC (%)	OPHI (%)	MET (%)	ALL (%)
AR1	4	93	1	-	-	-	2
AR2	39	20	9	-	1	-	32
FA1	66	32	-	-	-	-	2
FA2	52	5	-	4	1	29	10
FE1	45	55	-	-	-	-	-
FE2	56	14	-	1	-	1	29
ME1	50	22	1	-	-	5	23
ME2	41	21	2	-	-	11	24
ME3	48	17	1	1	-	6	28
ME4	36	16	1	1	3	17	28
ME5	39	14	2	2	-	19	25
GR1	3	3	-	5	-	20	70
GR2	4	2	-	10	-	27	57
MEL1	78	2	7	-	-	-	13
OM0	-	15	74	-	-	-	11
OM1	46	2	12	-	-	-	40
OM2	41	15	10	-	1	-	34
OM3	46	12	9	1	1	-	33
OM4	43	13	6	1	1	8	30
OM5	43	12	7	1	1	7	30
OM6	49	9	8	2	1	5	28
OM7	49	9	8	2	1	5	27
OM8	47	8	7	2	1	7	29
OM9	47	8	7	2	1	7	29
OM10	47	8	7	2	1	7	30
OM11	48	8	7	2	1	6	29
OM12	48	8	8	2	1	6	28
OM13	47	7	11	2	1	6	28
OM14	46	7	11	2	1	6	28
OR1	36	32	-	-	-	-	32
OR2	62	4	3	1	-	-	31
OR3	59	4	9	3	1	-	25
TR1	60	6	21	-	-	-	13

references therein). In this framework, this work focuses on how and to what extent the bedrock drained by the watersheds of the OGRB controls the chemical composition, mineralogy and magnetic susceptibility (χ) of stream sediments, and whether anthropogenic influence can be identified and assessed by these proxies. As analysis have been conducted on two different grain sizes (Sec. 2.2.1), Sec. 4.1 assesses the differences between the two aliquots, whereas the subsequent sections (4.2 to 4.5) focus on the building of an holistic approach in the identification of the main drivers of the OGRB stream sediments composition. Indeed, Sec. 4.2 is dedicated to the building and method validation of the ilr-balance framework through geochemical-mineralogical correlations, Sec. 4.3 to the interpretation of the natural lithological controls on sediment composition and Sec. 4.4 to the identification of anthropogenic signals related to historical.

4.1. Grain size effect analysis

Stream sediments were analysed in two aliquots sieved at <180 μm (A) and <2 mm (B), respectively (see Sec. 2.2.1). The spatial distribution of the A aliquot is largely controlled by basin lithology and morphology. Taking into consideration the A/B percentages (i.e., % of <180 μm; Fig. S5 in Supplementary Figures), finer sediments are predominantly concentrated in the central sector of the OGRB, where SHL lithologies dominate (Fig. 2) and the morphology is relatively flat compared to the basin edges.

To quantify the differences between analysis carried out on the two different grain sizes (Table 3), the median values of both aliquot A and B have been computed for all the considered elements and mineralogical phases, and the differences have been assessed as the relative difference between A and B medians $[(median_A - median_B)/median_B*100]$; therefore, positive results imply an enrichment in the considered component in the A aliquot, whereas negative values indicate the enrichment of the element or mineralogical phase in the B aliquot.

Geochemical comparison of the two aliquots reveals systematic

Table 3
Median values of geochemical and mineralogical parameters for the <180 μm (A) and <2 mm (B) aliquots, and their relative difference [=(median$_A$ − median$_B$)/median$_B$ × 100]. Positive values indicate enrichment in the A aliquot; negative values indicate enrichment in the B aliquot.

	A	B	Relative difference between medians (%)
χ (x 10^{-8} m^3/kg)	20.9	26.1	−19.9
LOI (wt.%)	11.5	11.0	4.68
SiO_2 (wt.%)	56.5	57.3	−1.35
TiO_2 (wt.%)	0.55	0.45	22.0
Al_2O_3 (wt.%)	10.9	10.1	7.51
Fe_2O_3 (wt.%)	4.87	4.87	−0.06
MnO (wt.%)	0.12	0.12	0.82
CaO (wt.%)	9.46	9.41	0.52
Na_2O (wt.%)	0.87	0.80	8.74
K_2O (wt.%)	1.89	1.79	5.62
P_2O_5 (wt.%)	0.11	0.10	8.99
MgO (wt.%)	1.65	1.56	5.96
V (ppm)	75.9	67.9	11.7
Cu (ppm)	30.7	27.6	11.1
Zn (ppm)	83.6	76.7	8.94
Ga (ppm)	14.3	13.4	6.54
Rb (ppm)	83.4	76.4	9.15
Sr (ppm)	243	236	2.64
Zr (ppm)	150	111	34.6
Ba (ppm)	304	285	6.53
Micas (%)	17	13	31
Quartz %	57	59	−3
Calcite (%)	13	13	−4
Chlorite group minerals (%)	9	9	-
Plagioclase (%)	5	6	−17

enrichment in the <180 μm fraction for several elements (Table 3). The largest relative differences between median values are observed for Zr (+34.6%), TiO_2 (+22.0%), Cu (+11.1%), V (+11.7%), whereas all other elements show a relative difference of medians below 10%. The strong enrichment of Zr in the A aliquot likely reflects its preferential concentration in heavy accessory phases reporting to the fine fraction. Cu (and Zn) is an element linked to mining activity in the OGRB (Sec. 2.1.3), and it is systematically higher in the A aliquot, consistent with the affinity of these metals for fine particles (e.g., Franceschelli et al., 1986).

.

Mineralogical differences between the two fractions are consistent with the geochemical patterns. The <180 μm aliquot shows a relative enrichment in micas of 30.8% compared to the B aliquot, whereas the latter is slightly enriched in quartz (+3.4%), which act as dilutants of the trace element signal in the coarser fraction.

Mass specific magnetic susceptibility median values are higher in the B aliquot (26.1 × 10^{-8} m^3/kg) compared to the A aliquot (20.9 × 10^{-8} m^3/kg). Raman spectroscopy of ferrimagnetic particles from high-χ samples (e.g., Fig. S2 in Supplementary Figures) identifies both magnetite and serpentine. The serpentine group minerals were not detected by XRD due to their concentration being below the detection limit. The higher χ in the B aliquot is therefore likely linked to the presence of coarse serpentine grains with magnetite inclusions, which are preferentially retained in the <2 mm fraction.

Overall, most elements show differences below 10% (except for TiO_2, Cu, V and Zr; see Table 3), indicating that the geochemical characteristics identified in this study are independent of the grain size fraction considered. The selection of two grain size fractions thus represents a complementary and analytically justified approach: the <2 mm fraction captures the bulk lithological signal of the basin, whilst the <180 μm fraction likely enhances the detection of anthropogenic inputs, as seen by the enrichment of Zn and Cu in the A aliquot. Retaining both in the analysis provides a more robust and complete characterization of the factors dominating sediment geochemistry in the OGRB.

4.2. Knowledge driven SBP of ilr-transformed geochemical data: building and method validation

Disentangling natural and anthropogenic inputs to the stream sediment composition requires a holistic approach. The method described in this section does not focus on singular elements but rather favours the use of a cluster of elements, which allows to combine information, leading to a more robust interpretation of the results. Elemental concentrations from stream sediment geochemical data, which are compositional, were clustered using the SBP applied to ilr-transformed data (Supplementary Table S1 and Fig. S6 in Supplementary Figures, for a summarized version see Table 4). These ilr-balances were selected using knowledge-driven criteria based on the lithologies of the area and the minerals that characterize those lithologies. Oxides were converted to elements.

The main lithologies outcropping within the OGRB can be summarized in five groups (excluding ALL, that are not lithologically characterized, and OPHI, which represent only a minor component): SND, SHL, CARB, MET and VOLC (Fig. 2). The building of the ilr-balances presented in Table 4 is based on the association of the various elements that primarily represent the main lithologies, also taking into consideration their mineralogical composition. This section focuses on the ilr-balances relevant for interpreting the stream sediment composition from the OGRB, rather than discussing all possible balances. The selected balances provide a solid framework for grouping elements according to lithological sources and characteristics of the basin (i.e., the mine exploitation) and for distinguishing natural versus anthropogenic contributions to the sedimentary load of the basin.

Ilr.1 is built with Ca and Sr at the numerator whereas all other considered elements are at the denominator (contributing to 74.5% of the variance of data), to assess the contribution of carbonate-rich lithologies (both CARB and SHL) to the samples. Ilr.3 (Si, Al, Na, K, Ba, Ga, Rb, Zr || Fe, V, Mn, Ti, Mg, P; accounting for 24.6% of data variability) divides elements linked to silicate minerals from element associated to Fe- and Mn-oxides, together with Mg and P, considering the high Fe content of the stream sediments analysed in this study compared to European baseline values (see Sec. 3.1.3). Mg was not included in the "carbonate component" of ilr.1 due to its almost ubiquitous presence in a variety of lithotypes (e.g., OPHI).

Sandstones and shales can be chemically distinguished on the logarithm of the SiO_2/Al_2O_3 contents, as seen with the SandClass system for the geochemical classification of terrigenous sands and shales proposed by Herron (1988), leading to the building of ilr.4 (Si, Zr || Al, Na, K, Ba, Ga, Rb; accounting for 8.11% of data variability). Ilr.4 infers also the

Table 4
Ilr transformations with their mean, median and variance (%). The symbol || separates elements at the numerator from those at the denominator of the log-ratio.

Ilr	Compositional parts within each balance	Mean	Median	Variance (%)
1	Ca, Sr || Si, Ti, Al, Fe, Mn, Na, K, P, Mg, Ba, Ga, Rv, V, Zr	0.90	1.04	74.5
2	Ca || Sr	3.95	3.98	5.4
3	Si, Al, Na, K, Ba, Ga, Rb, Zr || Fe, V, Mn, Ti, Mg, P	−0.07	−0.16	24.6
4	Si, Zr || Al, Na, K, Ba, Ga, Rb	2.09	2.08	8.11
5	Si || Zr	5.36	5.35	7.3
6	Na ||K, Al, Ba, Ga, Rb	1.88	1.88	27.6
7	K, Ba, Rb || Al, Ga	−0.23	−0.26	3.0
8	K, Rb || Ba	1.07	1.08	6.3
9	K || Rb	3.73	3.74	0.4
10	Al || Ga	5.86	5.86	0.6
11	Ti, Mn, V, Fe || Mg, P	−0.30	−0.30	7.5
12	Fe, Mn, V || Ti	−0.70	−0.73	4.7
13	Fe, V || Mn	0.42	0.42	6.1
14	Fe ||V	4.34	4.31	1.8
15	Mg ||P	2.14	2.12	12.6

influence of quartz and zircon rich lithologies, such as VOLC and MET (e.g., Rhyolitic lava flows outcropping in the Gretano sub-basin and Verrucano group; Annovi et al., 1980; Peccerillo, 2017 and references therein; Regione Toscana, 2022b), whereas the denominator includes those elements that can be ascribed to Al-rich minerals, such as feldspars and clay minerals. Ilr.6 (Na ||K, Al, Ba, Ga, Rb; 27.58% of data variability) and ilr.7 (K, Ba, Rb || Al, Ga; 3.00% of data variability) link, and possibly distinguish, the presence of feldspars and/or clay minerals, respectively. Ilr.12 (Fe, Mn, V || Ti, accounting to 4.68% of data variability) considers elements that are present in Fe- and Mn-oxides (e.g., Nesse, 1987) to infer a possible distinction in the contribution of magnetic susceptibility of samples; ilr.13 (Fe, V || Mn, contributing to 6.05%

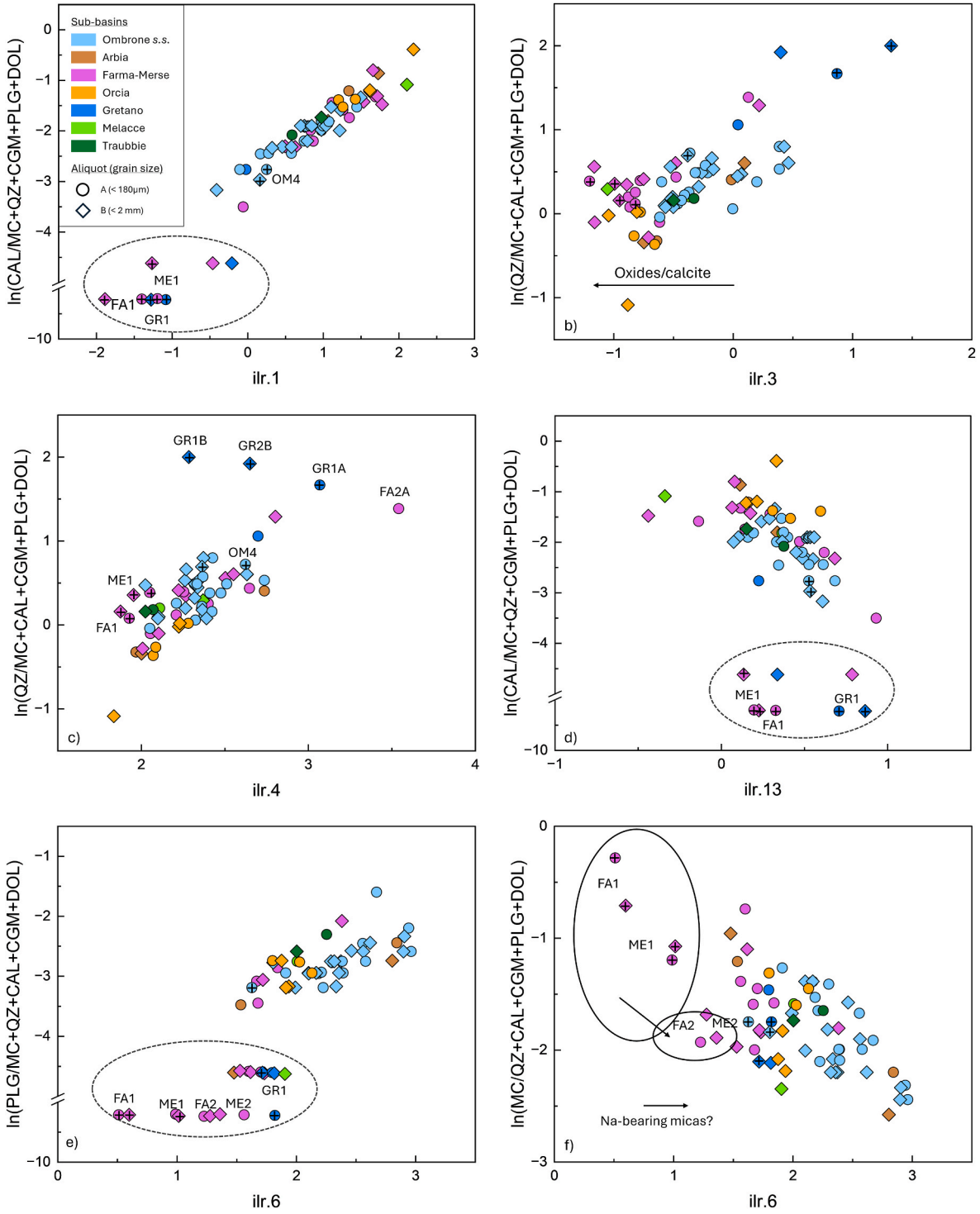

Fig. 7. Comparison between ilr and the log-ratios of the main mineralogical phases found in the OGRB. CAL = calcite; QZ = quartz; MC = mica; PLG = plagioclase; CGM = chlorite group minerals; DOL = dolomite. a) ilr.1 vs. ln(CAL/MC + QZ + CMG + PLG + DOL); b) ilr.3 vs. ln(QZ/MC + CAL + CGM + PLG + DOL); c) ilr.4 vs. ln(QZ/MC + CAL + CGM + PLG + DOL); d) ilr.13 vs. ln(CAL/MC + QZ + CMG + PLG + DOL); e) ilr.6 vs. ln(PLG/MC + QZ + CAL + CMG + DOL); f) ilr.6 vs. ln(MC/QZ + CAL + CMG + PLG + DOL). Samples where the mineral at the numerator is below detection limit of <3% are highlighted with dashed circles. Key control samples ME1, FA1, GR1 and OM4 have been highlighted with a "+" within their symbol and their label has been added when necessary. The label methodology and position of samples can be inferred in Fig. 1.

of data variability) is then built to take into consideration the presence of Mn-rich carbonates in the Verrucano group (MET in Fig. 2; Annovi et al., 1980).

To evaluate and validate the interpretative power of these ilr-balances, they are compared to the mineralogical composition, thereby linking geochemical signals to the main minerals in the collected stream sediments from their distributions in binary diagrams (Fig. 7). For the visualization of mineralogical data, an arbitrary content of 1% has been attributed to "minor" amounts (<3%) and 0.01% when the mineral content was below the detection limit (Supplementary Table S1). Considering that the mineralogical data are compositional data as well, each mineral phase is expressed as the natural logarithm of the ratio of a given mineral phase to all the other mineral phases present within the OGRB stream sediments (Sec. 2.2.3). Such log-ratios estimate the relative abundance of each mineral phase in the appropriate sample space; for example, a sample dominated by a single phase (e.g. quartz) would return a ratio >1, and thus a positive log-ratio, whereas the opposite is true for mineral phases making up <50% of the mineral assemblage (Fig. 7). The relationship between the ilrs and the mineral abundances has been analysed using the non-parametric Spearman correlation coefficients (ρ) and the associated significance level (p).

Ilr.1 is linearly positive corelated to the relative calcite abundance (Fig. 7a; $\rho = 0.96$, $p < 0.001$), with the only exception of samples (highlighted with a dashed circle) where this mineral is absent (hence estimated at 0.01 %). In the case of ME1, FA1 and GR1, samples do not show detectable plagioclase or dolomite, hence their ilr.1 values are below 0. Therefore, Ca and Sr contents in the OGRB samples are attributed primarily to the carbonate component of the lithologies present.

Both ilr.3 ($\rho = 0.67$, $p < 0.001$) and ilr.4 ($\rho = 0.69$, $p < 0.001$) positively correlate to the relative quartz abundance (Fig. 7b and c). In the first case, a shift toward more negative ilr.3 is attributed to the presence of Fe-rich minerals and/or Mn-bearing calcite (e.g., carbonates in the Verrucano group; Annovi et al., 1980) affecting samples in the Farma-Merse sub-basin, as suggested by the slightly negative correlation between ilr.13 and the calcite contents (Fig. 7d; $\rho = -0.56$; $p < 0.001$). The correlation between Mn and calcite affects more than the sole areas where the Verrucano groups is present (Farma-Merse and Gretano sub-basins), as the samples from the Ombrone and Orcia Rivers follow the same trend. Plagioclase and micas influence the correlation between ilr.4 and the relative quartz abundance, producing negative shifts from the trend, as elements linked to these mineralogical phases are at the denominator. Positive shifts are attributed to the presence of zircon, which is a common accessory phase of the Verrucano Group (Annovi et al., 1980).

A positive correlation is present between ilr.6 and relative plagioclase contents (Fig. 7e; $\rho = 0.83$; $p < 0.001$) in most samples. Samples from Farma and Merse display an increase in ilr.6 going from spring to mouth (i.e., from samples FA1 and ME1 to, respectively, FA2 and ME2), despite the absence of plagioclase. This increase might be attributed to lithologies of their catchments where the watersheds pass over the Verrucano metasediments (MET in Fig. 2) bearing Na-bearing micas (paragonite, Franceschelli et al., 1986; Giorgetti et al., 1998). However, ilr.6 vs relative mica abundances (Fig. 7f; $\rho = -0.58$, $p < 0.001$) contents highlights a negative corelation, meaning that the Farma and Merse sediments only show an increase in Na-bearing micas but not in the total mica content. The influence of Na-bearing micas can be inferred only from these samples, as going downstream the relative abundance of plagioclase strongly influences the relation to ilr.6.

These comparisons confirm that the selected ilr-balances capture meaningful mineralogical signals across the basin, reflecting carbonates, quartz, feldspars, clays, and accessory phases. Building on this validation, the ilr-balances can now be used to disentangle the natural (i.e., lithological) controls on sediment composition, which are first addressed in the following section, before evaluating potential anthropogenic inputs.

4.3. Natural signal analysis

To assess and further investigate the influence of bedrock lithologies to the chemistry and mineralogical composition of samples, ilr-balances were cross-plotted (Fig. 8), with the support of data retrieved from the watershed map and their lithological composition (Table 2); only the significant relations are discussed hereafter.

The comparison of ilr.1 and ilr.3 (Fig. 8a) highlights the strong influence of the local outcropping lithologies. Samples rich in calcite or quartz are discriminated, matching the spatially associated rock types. Specifically, the calcite-rich samples were collected from areas dominated by carbonate-rich lithologies (CARB and SHL see Fig. 2). In contrast, the quartz-rich samples were collected on quartzites, phyllites, and quartzose metaconglomerates (SND, VOLC (GR1), and MET). The majority of the samples plots along the mixing line between the calcite-rich and quartz-rich end-members, evidencing the dominant role of these two lithologies in controlling the chemical composition; it is interesting to note that the samples from the tributaries constitute the end-members, whereas the samples from the Ombrone River plot in the middle, acting as a homogenizing basin. A shift toward the left lower corner is attributed to the Mg and Fe enrichment that characterized some samples of the Farma-Merse sub-basin in relation to the contribution from OPHI (e.g., ME4; see Table 2 for the lithological composition and Supplementary Table S1 for mineralogical composition), as confirmed by the high χ values of samples lying in this area (i.e., FA1, ME1) that are related to the presence of Fe-bearing phases. Samples ME1 and ME4 are located in the proximity of mining sites (Fig. 4), suggesting that the mineralizations, as well as anthropogenic sources, influence their composition. These possible anthropogenic contributions will be better explored in Sec. 4.4.

A better constrain on the lithologies that influence the sedimentary load of the various sub-basins can be inferred by the comparison of ilr.6 and ilr.3 (Fig. 8b), which shows a clear distinction among the Ombrone, Orcia, Farma-Merse and Gretano sub-basins.

As seen in Sec. 4.2, there is a positive correlation between relative quartz contents and ilr.3 (Fig. 7b) and between relative plagioclase concentrations and ilr.6 (Figs. 7e and 8b). Taking into consideration the samples' location (Fig. 2) and the lithological composition of the watersheds (Table 2), we can further differentiate the influence of the main lithologies. The mixing trend affecting most of the samples is defined by two end-members: i) stream sediments from the Orcia and Farma-Merse sub-basins, and ii) samples from the Arbia (AR2) and the upper Ombrone River (OM0, OM1, OM2) (Fig. 8b). The former group is mainly affected by both CARB and SHL (see Table 2), whereas SND percentages are always below 5% (only exception is OR3 with 9%, but here SHL are more than 58%, therefore weighting more in the composition). The latter group is characterized by a decrease in the SND percentage downstream (74%, 12 % and 10% respectively for OM0, OM1 and OM2, and 9% for sample AR2).

Overall, sediment samples are discriminated by the ratio between SND and SHL + CARB, increasing from sample FE2B (belonging to the first group defined above) to the samples close to the spring of the Ombrone River (OM0, OM1, OM2) and AR2 (belonging to the second group). Therefore, ilr.3 vs. ilr.6 describes the influence and the proportions between these three lithologies in the majority of the sediment samples. The Gretano samples represent an outlier, as their watersheds are almost completely devoid of SHL or CARB (<5%) and their composition is mainly affected by VOLC and MET lithologies compared to the rest of the samples. Therefore, these samples point toward the MET + VOLC end-member for the OGRB samples. Samples ME4B, ME1 and FA1 lie outside from this trend: ME4B lies on ophiolitic sequences (OPHI) and is extremely enriched in Mg (and Fe) compared to all other samples (6.86 wt% and 6.27 wt%, respectively), which could explain the negative ilr.3 shift. Samples ME1 and FA1 are characterized by the highest Fe contents that have been highlighted for the whole Farma-Merse sample group (both ca. 8 wt%), but these are also the samples

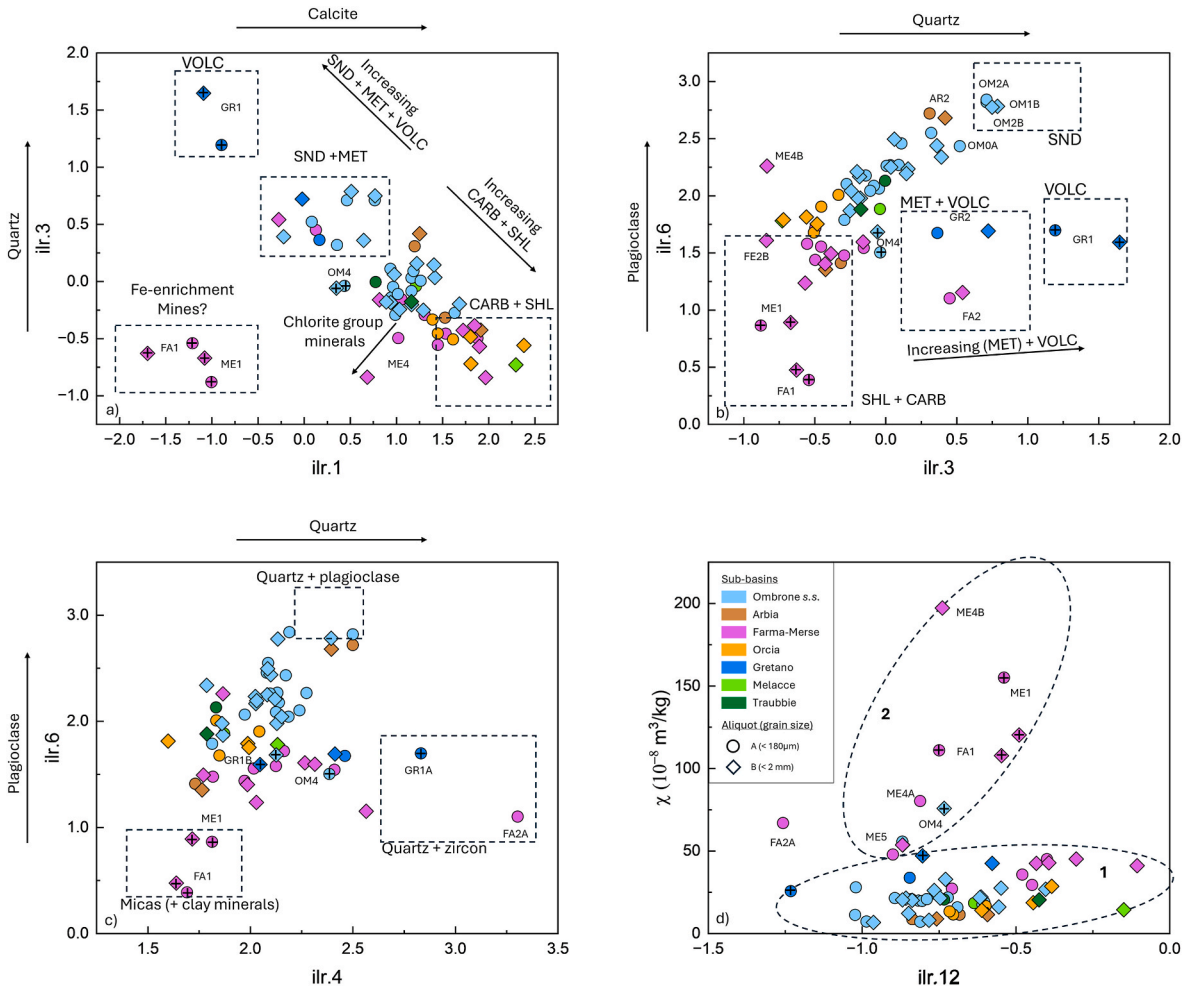

Fig. 8. Comparison between ilrs and against the χ of sediment samples. a) ilr.1 vs. ilr.3; b) ilr.3 vs. ilr.6; c) ilr.4 vs. ilr.6; d) ilr.12 vs. χ (*10^{-8} m^3/kg). Dashed boxes in all panels outline clusters representing natural compositional endmembers or anthropogenic anomalies, based on the combined interpretation of ilr-balances, mineralogical data, and χ measurements. References to the mineralogical phase dominating the ilr (based on Fig. 7 and Sec. 4.2) have been placed outside of the plot limits, with arrows indicating the direction of increasing mineral abundance. Similarly, increasing percentages of lithologies have been indicated with arrows within the plots. Key control samples ME1, FA1, GR1 and OM4 have been highlighted with a "+" within their symbol and their label has been added when necessary. The label methodology and position of samples can be inferred in Fig. 1.

with the highest Al_2O_3 contents (respectively, ca. 14 wt% and ca. 17 wt % in both aliquot A and B), reflecting the significant presence of phyllosilicates, which might have caused the negative ilr.6 shift. Sample FA2 is also influenced by the presence of MET within its watershed, hence its presence in the proximity of the Gretano samples. When considering ilr.3 vs. ilr.6, it is interesting to note that the Orcia, Farma-Merse and Gretano tributaries display distinctive compositions, that allow for the discrimination of their samples based on their chemistry. The Ombrone River sediments appear to be mainly affected by the presence of SND, with a composition that is variously influenced by the tributaries; indeed, the SHL-CARB contribution progressively increases downstream the main waterway, in relation to their relative abundance to the total outcropping lithologies.

Ilr.4 and ilr.6 (Fig. 8c) were used to better infer the silicate fraction starting from ilr.3 vs. ilr6. A shift of samples towards the lower left corner of the plot is influenced by their mica contents, due to the presence of Al in the denominator of both ilr.4 and ilr.6. Indeed, this corner is populated by samples containing more than 20% of mica (e.g., FA1, ME1). Considering that clay minerals are enriched in Al, K, Rb and Ba, their presence contributes to lower the values of both ilr.4 and ilr.6. Therefore, the lower left corner of Fig. 8c may also reflect the presence of clay minerals. Supporting this, samples FA1 and ME1 exhibit significant amounts of chlorite group minerals (ca. 10 %). The upper right corner is influenced by the presence of both plagioclase (increase in ilr.6) and quartz (increase in ilr.4). The majority of the OGRB stream sediments are a mixture of clay-minerals and plagioclase + quartz, with the exception of those where the silicate component is ascribed almost exclusively to quartz (i.e., Gretano samples and FA2). Even in this case, it is clear that the Farma-Merse and Gretano sub-basins insist on different lithologies compared to those that characterize the Orcia and Ombrone sub-basins. Furthermore, the A-aliquots (<180 μm) of GR1, GR2, and FA2 display high Zr contents (400, 220, and 960 ppm, respectively), likely reflecting the presence of zircon, producing a deviation from the general trend. The Ombrone River sediments are characterized by the highest plagioclase and quartz contents, whereas samples lying upon MET and VOLC lithologies are mainly influenced by the presence of quartz and zircon. The Orcia and Farma-Merse sediments' composition seems to be the most affected by the presence of micas, consistent with the mineralogical features of the bedrock lithologies characterizing their watersheds.

Conclusively, the comparison of ilrs confirms that the lithological proportions strongly control sediment chemistry, whereas localized anomalies indicate anthropogenic influence from historical mining.

4.4. Anthropogenic signal identification

The comparison between ilr.12 and mass specific magnetic susceptibility values (Fig. 8d) argue for the potential of χ as a quick proxy for anthropogenic contaminations (e.g., Scholger, 1998). Based on this graph, two samples' groups are highlighted: i) group 1, with lower median χ of 20.9 m^3/kg, and (ii) group 2, with a sharp increase in the χ/ilr.12 and a median χ of 94.0 m^3/kg. Samples pertaining to group 2 include both aliquots of FA1, ME1, ME4, ME5 and OM4, whereas all other samples fall within group 1. Sample FA2 has been removed from these considerations due to its combination of high χ but low ilr.12, placing it outside of the two defined groups. Based on this classification, the high-χ samples are predominantly located within the Merse-Farma sub-basin, except for sample OM4, which was collected immediately downstream of the sub-basin confluence along the Ombrone River. Notably, these samples originate from areas characterized by the "pyrite zone" (Dini, 2003) and ophiolitic lithologies (OPHI) that were historically exploited for iron (Figs. 2 and 4) as well as Cu and Zn (see Fig. S1 in Supplementary Figures). Some of the high-χ samples (e.g., ME1) were collected in areas where mine waste dumps are located (Benvenuti et al., 1997).

Other samples from the same sub-basin (e.g., FE2, ME3) do not exhibit similarly elevated χ values despite deriving from the same lithologies. This suggests that the specific magnetic susceptibility of group 2 may not solely reflect lithological controls, but also reflect a localized anthropogenic influence related to past mining activities. Accordingly, group 1 is interpreted as representative of the natural magnetic background of the basin, whereas group 2 likely captures superimposed signals from anthropogenic disturbances in specific areas.

Raman spectroscopy of ferrimagnetic particles from high-χ samples of group 2 (e.g., Fig. S2 in Supplementary Figures) identifies of both magnetite and serpentine. As the latter is not a magnetic mineral phase, it is assumed that the magnetic properties come from tiny magnetite inclusion. The morphology of most of these ferrimagnetic particles indicates a natural formation (Fig. S2 in Supplementary Figures), although these morphologies have been also found in mine waste dumps (Wang et al., 2023), thus further supporting the need for a multi-proxy approach combining χ with geochemical tracers.

Copper and Zn are two of the elements historically mined in the OGRB; therefore, both are used here as independent tracers to support the interpretation and validation of χ as a proxy for anthropogenic inputs in this river basin. To quantify the anthropogenic contribution of the mining activities on Fe, Cu, Zn in the two groups identified in Fig. 8d, we use the Enrichment Eactor (EF) computed as follows:

$$EF = \frac{\left(\frac{C_i}{C_{ref}}\right)_{sample}}{\left(\frac{C_i}{C_{ref}}\right)_{baseline}} \quad (1)$$

Where C_i represents the metal concentration and C_{ref} is the concentration of the reference element, represented by Al in this work as it is a conservative element (e.g., Barbieri, 2016). As the samples from group 1 represent the natural magnetic background, the median concentrations of Al_2O_3, Fe_2O_3, Cu and Zn which are, respectively, 10.2 wt%, 4.56 wt%, 27.6 ppm and 76.7 ppm, are used as the baseline values for the calculation of the EF in samples from group 2. Results are shown in Table 5.

EF_{Fe2O3} remains constant at unity for all the samples, due to the general coupling of Fe_2O_3 and Al_2O_3 even in the samples with the highest Fe contents (e.g. ME1 and FA1 both aliquots, Supplementary Table S1). Benvenuti et al. (1997) reported the presence of Al-oxyhydroxides in mine waste dumps of the nearby Boccheggiano mining district, which may further buffer the EF_{Fe2O3}.

Results highlight moderate enrichment (EF > 2; Barbieri, 2016) in Cu in samples ME1B and ME4A, and a significant enrichment (EF > 5; Barbieri, 2016) in ME1A, whereas Zn is significantly enriched in both aliquots of ME1. The enrichment in ME1 is compatible with the location of this sampling point in the proximity of a mine waste dump site (Gabbellino; Benvenuti et al., 1997).

Table 5
EFs computed for Fe_2O_3, Cu and Zn in samples from group 2 identified in Fig. 8d. Median values for Al_2O_3, Cu and Zn from samples from group 1 (Fig. 8d) have been used as the baseline for the EF computation.

Sample	EF_{Fe2O3}	EF_{Cu}	EF_{Zn}
FA1A	1	1	1
FA1B	1	1	1
ME1A	1	6	10
ME1B	1	4	6
ME4A	1	2	1
ME4B	1	1	1
ME5A	1	1	1
ME5B	1	1	1
OM4A	1	1	1
OM4B	1	1	1

The virtual absence of enrichment in either Cu and Zn in all but few samples suggests that the anthropogenic signal related to past mining activities is spatially restricted to areas in close proximity to former mining sites and mine waste dumps, and its impact in other parts of the basin, although detectable, does not significantly alter the natural geochemical baseline of the broader OGRB, compatible with the generally low absolute χ values measured in the sediment samples.

Overall, results confirm that magnetic susceptibility effectively distinguishes natural Fe-bearing mineral phases from localized anthropogenic inputs, thus representing a valuable screening tool within multi-proxy frameworks for the assessment of human influences on stream sediments in the OGRB. In this context, it is interesting to point out that magnetic susceptibility and ilr seem to be able to detect the effect of human inputs even where EFs remain relatively low.

5. Conclusions

The integration of CoDA-based ilr-balances, mineralogical log-ratios and mass specific magnetic susceptibility provides a coherent framework for the characterization of stream sediment composition in the OGRB, as seen in Sec. 4.2 to 4.4. Each proxy contributes in the disentanglement of the drivers of the OGRB sediments composition: ilr-balances allow for the identification of the main lithological signals, mineralogical log-ratios anchor these signals to specific mineral phases, and magnetic susceptibility, supported by data on Cu and Zn, offers a rapid indicator of Fe-bearing phase distribution sensitive to both natural (OPHI contribution) and anthropogenic (mining related) inputs. This multi-proxy approach shows that geochemical patterns are primarily controlled by lithology at the basin scale, whereas mining-related anomalies appear as localized deviations from the natural background. Despite the relatively limited number of samples (33) compared to the basin extent (ca. 3500 km^2), the sampling strategy allows to capture the main lithological contrasts between the various sectors of the OGRB (western, central and eastern), as well as anthropogenic influences in the Farma-Merse sub-basin. Moreover, the CoDA approach help to overcome the limitations of a landscape-scale sampling. By focusing on log-ratio balances rather than absolute concentrations, we can robustly identify the geochemical fingerprint of each lithological domain, ensuring that the identified patterns are statistically sound despite the sample size.

Therefore, the results represent an effective first-order assessment of sediment characteristics and provenance.

Overall, this study shows that ilr-transformed CoDA approaches provide an integrative preliminary framework for understanding stream sediment composition, linking geochemistry to mineralogy, tracing lithological sources, and detecting anthropogenic influences. A further advantage is related to the consideration of the whole compositions,

thus taking better into account the complex processes affecting the joint transfer of elements among different matrices. By explicitly linking compositional geochemical balances to sediment mineralogy, this study demonstrates that lithological controls dominate stream sediment chemistry at the basin scale, whereas mining-related inputs emerge as localized perturbations superimposed on the natural geochemical background. This distinction is critical for interpreting sediment geochemical data in historically exploited terrains.

CRediT authorship contribution statement

Francesca Giannetti: Conceptualization, Data curation, Formal analysis, Investigation, Methodology, Validation, Visualization, Writing – original draft, Writing – review & editing. **Caterina Gozzi:** Conceptualization, Data curation, Formal analysis, Investigation, Methodology, Supervision, Validation, Visualization, Writing – original draft, Writing – review & editing. **Gerd Rantitsch:** Formal analysis, Methodology, Resources, Validation, Writing – review & editing. **Stefania Venturi:** Conceptualization, Data curation, Investigation, Methodology, Supervision, Validation, Visualization, Writing – review & editing. **Riccardo Avanzinelli:** Conceptualization, Data curation, Investigation, Methodology, Supervision, Validation, Writing – review & editing. **Robert Scholger:** Formal analysis, Resources, Validation, Writing – review & editing. **Claudio Natali:** Data curation, Supervision, Validation, Writing – review & editing. **Giovanni Orazio Lepore:** Formal analysis, Validation, Writing – review & editing. **Marta Morana:** Formal analysis, Validation, Writing – review & editing. **Valentina Rimondi:** Validation, Writing – review & editing. **Antonella Buccianti:** Conceptualization, Data curation, Funding acquisition, Investigation, Methodology, Resources, Supervision, Validation, Writing – review & editing.

Declaration of competing interest

The authors declare that they have no known competing financial interests or personal relationships that could have appeared to influence the work reported in this paper.

Acknowledgement and funding

This project was funded under the National Recovery and Resilience Plan (NRRP), Mission 4 Component 2 Investment 1.4 — Call for tender No. 3138 of 16 December 2021, rectified by Decree no. 3175 of 18 December 2021 of Italian Ministry of University and Research (MUR) funded by the European Union – NextGenerationEU. Award Numbers: Project codes CN_00000033 and CN_00000013, Concession Decree No. 1034 of 17 June 2022 adopted by the Italian Ministry of University and Research, CUP: B83C22002910001 and B83C22002830001, Project titles “National Biodiversity Future Centre — NBFC” (A.B, C.G, S.V., F.G. and V.R.) and “National Centre for HPC , Data and Quantum Computing” (A.B). X-ray diffraction measurements were performed at Centro di Servizi di Cristallografia Strutturale (CRIST), University of Florence. We thank the two anonymous reviewers for their suggestions and critical reviews that greatly helped to improve the paper.

Appendix A. Supplementary data

Supplementary data to this article can be found online at https://doi.org/10.1016/j.apgeochem.2026.106921.

Data availability

Data are available within the article and its supplementary materials (Supplementary Table S1 and Supplementary Figures).

References

Aitchison, J., 1982. The statistical analysis of compositional data. J. Roy. Stat. Soc. B 44 (2), 139–160. https://doi.org/10.1111/j.2517-6161.1982.tb01195.x.
Aitchison, J., 1986. The Statistical Analysis of Compositional Data. Chapman and Hall.
Annovi, A., Fontana, D., Gelmini, R., Gorgoni, C., Sighinolfi, G., 1980. Geochemistry of carbonate rocks and ferruginous horizons in the Verrucano in southern Tuscany - paleoenvironmental and paleogeographic implications. Palaeogeogr. Palaeoclimatol. Palaeoecol. 30, 1–16. https://doi.org/10.1016/0031-0182(80)90046-2.
ARPAT, 2014. Monitoraggio ambientale del sistema Merse - campiano. Elaborazione Ed Interpretazione Dei Risultati Dell’Attività Di Monitoraggio. Anno 2013. Dipartimento Provinciale ARPAT di Grosseto - Regione Toscana (in italian).
ARPAT, 2017. Monitoraggio ambientale del sistema Merse - campiano. Elaborazione Ed Interpretazione Dei Risultati Dell’Attività Di Monitoraggio. Anni 2014–2015. Dipartimento Provinciale ARPAT di Grosseto - Regione Toscana (in italian).
Auzende, A.L., Daniel, I., Reynard, B., Lemaire, C., Guyot, F., 2004. High-pressure behaviour of serpentine minerals: a Raman spectroscopic study. Phys. Chem. Miner. 31, 269–277. https://doi.org/10.1007/s00269-004-0384-0.
Barbieri, M., 2016. The importance of enrichment factor (EF) and geoaccumulation index (Igeo) to evaluate the soil contamination. J. Geol. Geophys. 5 (1), 1–4. https://doi.org/10.4172/2381-8719.1000237.
Beck, H.E., Zimmermann, N.E., McVicar, T.R., Vergopolan, N., Berg, A., Wood, E.F., 2018. Present and future Köppen-Geiger climate classification maps at 1-km resolution. Sci. Data 5 (1), 180214. https://doi.org/10.1038/sdata.2018.214.
Benvenuti, M., Mascaro, I., Corsini, F., Lattanzi, P., Parrini, P., Tanelli, G., 1997. Mine waste dumps and heavy metal pollution in abandoned mining district of Boccheggiano (Southern Tuscany, Italy). Environ. Geol. 30 (3), 238–243. https://doi.org/10.1007/s002540050152.
Bonciani, F., Callegari, I., Conti, P., Cornamusini, G., Carmignani, L., 2005. Neogene post-collisional evolution of the internal Northern Apennines: insights from the upper Fiora and Albegna valleys (Mt. Amiata geothermal area, southern Tuscany). Boll. Soc. Geol. Ital. 3 (Special Issue), 103–118.
Brogi, A., Lazzarotto, A., Liotta, D., 2005. Structural features of southern Tuscany and geological interpretation of the CROP 18 Seismic Reflection Survey (Italy). Boll. Soc. Geol. Ital. 3, 213–236.
Brogi, A., Liotta, D., 2008. Highly extended terrains, lateral segmentation of the substratum, and basin development: the middle-late Miocene Radicondoli Basin (inner northern Apennines, Italy). Tectonics 27 (5). https://doi.org/10.1029/2007TC002188.
Carmignani, L., Conti, P., Cornamusini, G., Meccheri, M., Crescenti, U., 2004. The internal Northern Apennines, the northern Tyrrhenian sea and the Sardinia-Corsica block. Geology of Italy. Special Volume, Italian Geological Society, IGC 32, 59–77.
Carmignani, L., Decandia, F.A., Fantozzi, P.L., Lazzarotto, A., Liotta, D., Meccheri, M., 1994. Tertiary extensional tectonics in Tuscany (northern Apennines, Italy). Tectonophysics 238 (1–4), 295–315. https://doi.org/10.1016/0040-1951(94)90061-2.
Cavalieri, S., 2001. Ombrone grossetano. In: Agenzia Nazionale per La Protezione Dell'Ambiente (A Cura Di), Primo Rapporto Sinanet Sulle Acque. Stato dell'Ambiente. Parte B 3/2001). Roma: ANPA (in italian).
Chiarantini, L., Benvenuti, M., Beutel, M., Costagliola, P., Covelli, S., Gabbani, G., Lattanzi, P., Pandeli, E., Paolieri, M., Petranich, E., Rimondi, V., 2016. Mercury and arsenic in stream sediments and surface waters of the Orcia River basin, southern Tuscany, Italy. Water, Air, Soil Pollut. 227 (11), 408. https://doi.org/10.1007/s11270-016-3110-x.
Cipriani, C., Tanelli, G., 1983. Risorse minerarie ed industria estrattiva in Toscana. Atti e Memorie Accademia di Scienze e Lettere La Colombaria 28, 241–283 (in italian).
Coelho, A.A., 2018. TOPAS and TOPAS-Academic: an optimization program integrating computer algebra and crystallographic objects written in C++. Applied Crystallography 51 (1), 210–218. https://doi.org/10.1107/S1600576718000183.
Conticelli, S., Laurenzi, M.A., Giordano, G., Mattei, M., Avanzinelli, R., Melluso, L., Tommasini, S., Boari, E., Cifelli, F., Perini, G., Peccerillo, A., 2010. Leucite-bearing (kamafugitic/leucititic) and-free (lamproitic) ultrapotassic rocks and associated shoshonites from Italy: constraints on petrogenesis and geodynamics. J. Virtual Explor. 36 (20), 1–95.
Cornamusini, G., Foresi, L.M., Massa, G., Bonciani, F., Callegari, I., Da Prato, S., Ielpi, A., 2011. The Miocene successions of the Fiora Hills: considerations about the development of the minor basins of Southern Tuscany. Ital. J. Geosci. 130 (3), 404–424. https://doi.org/10.3301/IJG.2011.17.
D. Lgs 152/06-Legislative Decree 152, 2006. Norme in Materia Ambientale Gazzetta Ufficiale No. 88. Italian Ministry of the Environment, p. 425 (in italian).
Dinelli, E., Cortecci, G., Lucchini, F., Zantedeschi, E., 2005. Sources of major and trace elements in the stream sediments of the Arno river catchment (northern Tuscany, Italy). Geochem. J. 39 (6), 531–545. https://doi.org/10.2343/geochemj.39.531.
Dini, A., 2003. Ore deposits, industrial minerals and geothermal resources. Period. Mineral. 72 (2), 41–52.
Dini, A., 2017. Miniere e minerali del Distretto mercurifero del Monte Amiata. In: Principe, C., Lavorini, G., Vezzoli, L. (Eds.), Il Vulcano Di Monte Amiata, pp. 343–369 (in italian).
Dini, A., Giannelli, G., Puxeddu, M., Ruggieri, G., 2005. Origin and evolution of Pliocene-Pleistocene granites from the Larderello geothermal field (Tuscan Magmatic Province, Italy). Lithos 81, 1–31. https://doi.org/10.1016/j.lithos.2004.09.002.
Dini, A., Rielli, A., Di Giuseppe, P., Ruggieri, G., Boschi, C., 2024. The ophiolite-hosted Cu-Zn VMS deposits of tuscany (Italy). Minerals 14 (3), 273. https://doi.org/10.3390/min14030273.
Dini, A., Westerman, D.S., Innocenti, F., Rocchi, S., 2008. Magma emplacement in a transfer zone: the Miocene mafic Orano dyke swarm of Elba Island, Tuscany, Italy.

In: Thomson, K., Petford, N. (Eds.), Structure and Emplacement of High-Level Magmatic Systems, 302. Geological Society, London, pp. 131–148. https://doi.org/10.1144/SP302.10.
Diodato, N., Ljungqvist, F.C., Fiorillo, F., Bellocchi, G., 2023. A framework for modelling emergent sediment loss in the Ombrone River Basin, central Italy. PLoS Water 2 (2), e0000072. https://doi.org/10.1371/journal.pwat.0000072.
Egozcue, J.J., Gozzi, C., Buccianti, A., Pawlowsky-Glahn, V., 2024. Exploring geochemical data using compositional techniques: a practical guide. J. Geochem. Explor. 258, 107385. https://doi.org/10.1016/j.gexplo.2024.107385.
Egozcue, J.J., Pawlowsky-Glahn, V., Mateu-Figueras, G., Barcelo-Vidal, C., 2003. Isometric logratio transformations for compositional data analysis. Math. Geol. 35 (3), 279–300. https://doi.org/10.1023/A:1023818214614.
Egozcue, J.J., Pawlowsky-Glahn, V., 2005. Groups of parts and their balances in compositional data analysis. Math. Geol. 37 (7), 795–828. https://doi.org/10.1007/s11004-005-7381-9.
Esri, 2025a. ArcGIS Pro [software], Version 3.x. https://www.esri.com.
Esri, 2025b. ArcGIS Pro Spatial Analyst extension: Hydrology and Spatial Analyst toolsets [software tools]. Esri Inc. Available from: https://pro.arcgis.com/en/pro-app/latest/tool-reference/spatial-analyst/an-overview-of-the-spatial-analyst-toolbox.htm.
Faměra, M., Matys Grygar, T., Elznicová, J., Grison, H., 2018. Geochemical normalization of magnetic susceptibility for investigation of floodplain sediments. Environ. Earth Sci. 77 (5), 189. https://doi.org/10.1007/s12665-018-7371-0.
Finetti, I.R., Boccaletti, M., Bonini, M., Del Ben, A., Geletti, R., Pipan, M., 2001. Crustal section based on CROP seismic data across the North Tyrrhenian–Northern Apennines–Adriatic Sea. Tectonophysics 343, 135–163. https://doi.org/10.1016/S0040-1951(01)00141-X.
Finetti, I.R., Boccaletti, M., Bonini, M., Del Ben, A., Pipan, M., Prizzon, A., 2005. Chapter 8 - lithospheric tectono-stratigraphic setting of the Ligurian Sea–Northern Apennines–Adriatic Foreland from integrated CROP seismic data. In: Finetti, I. (Ed.), CROP Project—Deep Seismic Exploration of the Central Mediterranean and Italy, Atlases in Geoscience. Elsevier B.V, pp. 119–158.
Franceschelli, M., Leoni, L., Memmi, I., Puxeddu, M., 1986. Regional distribution of Al-silicates and metamorphic zonation in the low-grade Verrucano metasediments from the northern Apennines, Italy. J. Metamorph. Geol. 4 (3), 309–321.
Frangipane, A., Paris, E., 1994. Long-Term Variability of Sediment Transport in the Ombrone River Basin (Italy), 224. IAHS Publications-Series of Proceedings and Reports-Intern Assoc Hydrological Sciences, pp. 317–324.
Frankowski, M., Zioła, A., Siepak, M., Siepak, J., 2008. Analysis of heavy metals in particular granulometric fractions of bottom sediments in the Mała Wełna River (Poland). SRM 54 (118), 19.
Giorgetti, G., Goffe, B., Memmi, I., Nieto, F., 1998. Metamorphic evolution of Verrucano metasediments in Northern Apennines; new petrological constraints. Eur. J. Mineral 10 (6), 1295–1308.
Gozzi, C., 2025. Environmental changes in river chemistry: a compositional approach for effective monitoring and management. Sci. Total Environ. 972, 179074. https://doi.org/10.1016/j.scitotenv.2025.179074.
Gozzi, C., Graziano, R.S., Frondini, F., Buccianti, A., 2018. Innovative monitoring tools for the complex spatial dynamics of river chemistry: case study for the Alpine region. Environ. Earth Sci. 77 (16), 579. https://doi.org/10.1007/s12665-018-7756-0.
Gozzi, C., Templ, M., Buccianti, A., 2024. Robust CoDA balances and the role of the variance in complex riverine geochemical systems. J. Geochem. Explor. 259, 107438. https://doi.org/10.1016/j.gexplo.2024.107438.
Gray, J.E., Rimondi, V., Costagliola, P., Vaselli, O., Lattanzi, P., 2014. Long-distance transport of Hg, Sb, and as from a mined area, conversion of Hg to methyl-Hg, and uptake of Hg by fish on the Tiber River basin, west-central Italy. Environ. Geochem. Health 36 (1), 145–157. https://doi.org/10.1007/s10653-013-9525-z.
Griffioen, J., Felder, M., Molenaar, N., Spijker, J., Hoving, A., 2025. Sediment mineralogy and geochemistry. In: Geology of the Netherlands, second ed. Amsterdam University Press, pp. 493–533. https://doi.org/10.2307/jj.27435714.17.
Halamić, J., Peh, Z., Bukovec, D., Miko, S., Galović, L., 2001. A factor model of the relationship between stream sediment geochemistry and adjacent drainage basin lithology, Medvednica Mt., Croatia. Geol. Croat. 54 (1), 37–51.
Herron, M.M., 1988. Geochemical classification of terrigenous sands and shales from core or log data. J. Sediment. Res. 58 (5), 820–829. https://doi.org/10.1306/212F8E77-2B24-11D7-8648000102C1865D.
Kirkwood, C., Everett, P., Ferreira, A., Lister, B., 2016. Stream sediment geochemistry as a tool for enhancing geological understanding: an overview of new data from south west England. J. Geochem. Explor. 163, 28–40. https://doi.org/10.1016/j.gexplo.2016.01.010.
Köppen, W.P., 1931. Grundriss Der Klimakunde. W. de Gruyter.
Liu, X., Wang, W., Pei, Y., Yu, P., 2020. A knowledge-driven way to interpret the isometric log-ratio transformation and mixture distributions of geochemical data. J. Geochem. Explor. 210, 106417. https://doi.org/10.1016/j.gexplo.2019.106417.
Liu, Y., Zhou, K., Carranza, E.J.M., 2018. Compositional balance analysis for geochemical pattern recognition and anomaly mapping in the western Junggar region, China. Geochem. Explor. Environ. Anal. 18, 263–276. https://doi.org/10.1144/geochem2017-050.
Marroni, M., Moratti, G., Costantini, A., Conticelli, S., Benvenuti, M.G., Pandolfi, L., Bonini, M., Cornamusini, G., Laurenzi, M.A., 2015. Geology of the Monte Amiata region, southern Tuscany, central Italy. Ital. J. Geosci. 134 (2), 171–199. https://doi.org/10.3301/IJG.2015.13.
Martini, I.P., Sagri, M., 1993. Tectono-sedimentary characteristics of late Miocene-Quaternary extensional basins of the Northern Apennines, Italy. Earth Sci. Rev. 34 (3), 197–233. https://doi.org/10.1016/0012-8252(93)90034-5.
Monaci, F., Ancora, S., Bianchi, N., Bonini, I., Paoli, L., Loppi, S., 2021. Combined use of native and transplanted moss for post-mining characterization of metal(loid) river contamination. Sci. Total Environ. 750, 141669. https://doi.org/10.1016/j.scitotenv.2020.141669.
Najafian, T., Mokhtari, A.R., Albanese, S., 2023. Is the pathway length of sediments relevant to assess the background value in stream sediment geochemical exploration? J. Geochem. Explor. 253, 107278. https://doi.org/10.1016/j.gexplo.2023.107278.
Nesse, W.D., 1987. Introduction to optical mineralogy. Appl. Opt. 26 (18), 3739.
Pandeli, E., 2008. La Pianura Di Firenze-Prato-Pistoia Nel Quadro Dell'Evoluzione Geologica Dell'Appennino Settentrionale. Atti del Convegno "Un Piano per La Piana: Idee E Progetti per Un Parco. Polo Scientifico e Tecnologico di Sesto Fiorentino, Università di Firenze (in italian).
Pawlowsky-Glahn, V., Egozcue, J.J., Tolosana-Delgado, R., 2015. Modeling and Analysis of Compositional Data. John Wiley & Sons.
Pawlowsky-Glahn, V., Egozcue, J.J., 2001. Scaling stratigraphic events using extreme occurrences. International Statistical Institute Bulletin Book 2, 473–476.
Peccerillo, A., 2017. The tuscany Province. In: Cenozoic Volcanism in the Tyrrhenian Sea Region. Advances in Volcanology. Springer, Cham. https://doi.org/10.1007/978-3-319-42491-0_2.
Peeters, L., 2014. A background color scheme for Piper plots to spatially visualize hydrochemical patterns. Groundwater 52, 2–6. https://doi.org/10.1111/gwat.12118.
Toscana, Regione, 2012. Banca Dati risorse minerarie (BD_RIMI) [Database]. Regione Toscana GeoNetwork. https://www502.regione.toscana.it/geonetwork/srv/api/records/r_toscan:69506fc1-d275-441f-af4d-d17aa310c4a4.
Toscana, Regione, 2021. Hydrographic Digital Terrain Model (HDTM). Regione Toscana [data set]. https://www502.regione.toscana.it/geonetwork/srv/search?keyword=modello%20digitale%20del%20territorio.
Regione Toscana, 2022a. Banca Dati Attività Estrattive Della Regione Toscana. https://cave.regione.toscana.itConsulted. (Accessed 17 January 2025).
Regione Toscana, 2022b. Legenda Unità Geologiche e Depositi Superficiali (Scala 1: 250000). Regione Toscana [data set]. https://www.regione.toscana.it/-/banche-dati-cartografia-geologica.
Reimann, C., Melezhik, V., 2001. Metallogenic provinces, geochemical provinces and regional geology—what causes large-scale patterns in low density geochemical maps of the C-horizon of podzols in Arctic Europe? Appl. Geochem. 16 (7–8), 963–983. https://doi.org/10.1016/S0883-2927(00)00064-0.
Salminen, R., Batista, M.J., Bidovec, M., Demetriades, A., De Vivo, B., De Vos, W., Duris, M., Gilucis, A., Gregorauskiene, V., Halamic, J., Heitzmann, P., Lima, A., Jordan, G., Klaver, G., Klein, P., Lis, J., Locutura, J., Marsina, K., Mazreku, A., O'Connor, P.J., Olsson, S.Å., Ottesen, R.-T., Petersell, V., Plant, J.A., Reeder, S., Salpeteur, I., Sandström, H., Siewers, U., Steenfelt, A., Tarvainen, T., 2005. In: Geochemical Atlas of Europe. Part 1: Background Information, Methodology and Maps. Geological Survey of Finland, Espoo [data set].
Schmidt, A., Yarnold, R., Hill, M., Ashmore, M., 2005. Magnetic susceptibility as proxy for heavy metal pollution: a site study. J. Geochem. Explor. 85 (3), 109–117. https://doi.org/10.1016/j.gexplo.2004.12.001.
Scholger, R., 1998. Heavy metal pollution monitoring by magnetic susceptibility measurements applied to sediments of the river Mur (Styria, Austria). Eur. J. Environ. Eng. Geophys. 3, 25–37.
Shebanova, O.N., Lazor, P., 2003. Raman spectroscopic study of magnetite (FeFe2O4): a new assignment for the vibrational spectrum. J. Solid State Chem. 174 (2), 424–430. https://doi.org/10.1016/S0022-4596(03)00294-9.
Thió-Henestrosa, S., Martín-Fernández, J.A., 2005. Dealing with compositional data: the freeware CoDaPack. Math. Geol. 37 (7), 773–793. https://doi.org/10.1007/s11004-005-7379-3.
Vaitkus, A., Merkys, A., Sander, T., Quirós, M., Thiessen, P.A., Bolton, E.E., Gražulis, S., 2023. A workflow for deriving chemical entities from crystallographic data and its application to the Crystallography Open Database. J. Cheminf. 15. https://doi.org/10.1186/s13321-023-00780-2.
Villani, L., Castelli, G., Yimer, E.A., Chawanda, C.J., Nkwasa, A., Van Schaeybroeck, B., Penna, D., van Griensven, A., Bresci, E., 2024. Impacts of climate change and vegetation response on future aridity in a Mediterranean catchment. Agric. Water Manag. 299, 108878. https://doi.org/10.1016/j.agwat.2024.108878.
Wang, G., Liu, X., Song, L., Ma, X., Chen, W., Qiao, J., 2023. Micro-structure and morphology of tailings sand under different oxidation and acidification degree. Sci. Rep. 13 (1), 981. https://doi.org/10.1038/s41598-022-26130-0.
Wang, H., Yuan, Z., Cheng, Q., Zhang, S., Sadeghi, B., 2022. Geochemical anomaly definition using stream sediments landscape modeling. Ore Geol. Rev. 142, 104715. https://doi.org/10.1016/j.oregeorev.2022.104715.
Webb, P.C., Potts, P.J., Thompson, M., Gowing, C.J.B., 2022. GeoPT50—AN INTERNATIONAL PROFICIENCY TEST FOR ANALYTICAL GEOCHEMISTRY LABORATORIES.
Wentworth, C.K., 1922. A scale of grade and class terms for clastic sediments. J. Geol. 30 (5), 377–392. https://doi.org/10.1086/622910.
Wilber, W.G., Hunter, J.V., 1979. The impact of urbanization on the distribution of heavy metals in bottom sediments of the Saddle River 1. JAWRA Journal of the American Water Resources Association 15 (3), 790–800. https://doi.org/10.1111/j.1752-1688.1979.tb00397.x.
Xie, S., Cheng, Q., Xing, X., Bao, Z., Chen, Z., 2010. Geochemical multifractal distribution patterns in sediments from ordered streams. Geoderma 160 (1), 36–46. https://doi.org/10.1016/j.geoderma.2010.01.009.